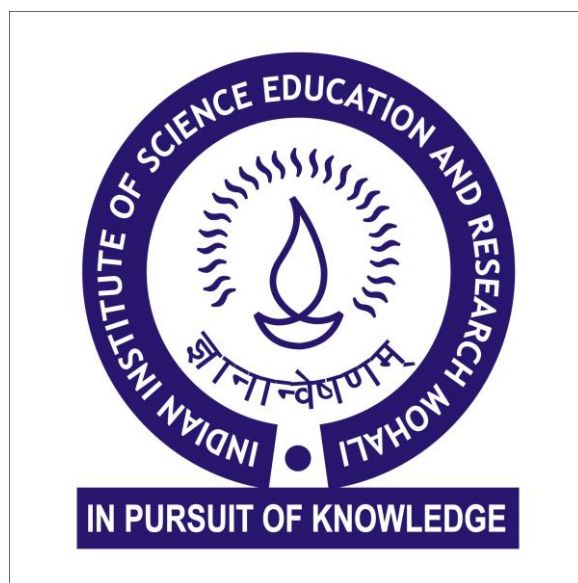


Palladium Nanoparticles Supported on Nitrogen doped Reduced Graphene Oxide (Pd/NrGO) for Fuel Cell Reactions

Anshul
MS18193

*A dissertation submitted for the partial fulfilment of BS-MS dual degree in
Science*



Indian Institute of Science Education and Research, Mohali,

April, 2023

Certificate of Examination

This is to certify that the dissertation titled “ **Palladium Nanoparticles Supported on Nitrogen doped Reduced Graphene Oxide (Pd/NrGO) for Fuel Cell Reactions** ” submitted by **Anshul** (Reg. No. MS18193) for the partial fulfillment of BS- MS Dual Degree programme of the institute, has been examined by the thesis committee duly appointed by the institute. The committee finds the work done by the candidate satisfactory and recommends that the report be accepted. satisfactory and recommends that the report be accepted.

Dr. Suman K. Burman

Dr. Sanchita Sengupta

Dr. Ujjal K. Gautam

Dr. Ujjal K. Gautam
(Supervisor)

Dated: 10-04-2023

Declaration

The work presented in this dissertation has been carried out by me under the guidance of **Dr.Ujjal K. Gautam** at the Indian Institute of Science Education and Research, Mohali.

This work has not been submitted in part or in full for a degree, a diploma, or a fellowship to any other university or institute. Whenever contributions of others are involved, every effort is made to indicate this clearly, with due acknowledgement of collaborative research and discussions. This thesis is a bonafide record of original work done by me and all sources listed within have been detailed in the bibliography.

ANSHUL

(Candidate)

Dated: 10-04-2023

In my capacity as the supervisor of the candidates project work, I certify that the above statements by the candidate are true to the best of my knowledge.

Dr. Ujjal K. Gautam

(Supervisor)

Dated: 10-04-2023

Acknowledgements

First and foremost, from the innermost core of my heart I express my profound sense of respect and honor to my supervisor, moreover my best academic guide **Dr. Ujjal K. Gautam**, Department of Chemical Sciences, Indian Institute of Science Education and Research (IISER) Mohali, for his inspiration, benign cooperation, excellent guidance, exemplary supervision, timely criticism, useful comments, remarks and engagement throughout the course of my project. He gave me so much freedom to think and without his persistent care and assistance, this dissertation would not have been possible.

I would like to thank my committee members Dr. Suman K. Burman and Dr. Sanchita Sengupta for their comprehensive advice and encouragement. I am pleased to acknowledge Prof. J Gourishankar and to Prof. Dr. Sanjay Singh (HOD, Department of Chemical Sciences, IISERM) for providing supreme research facilities in IISER Mohali.

I would like to express my sincere thanks to Ms. Komalpreet Kaur for her passionate guidance and valuable encouragement. She guided me throughout my project and I am gratefully indebted to her valuable comments and friendly counseling. I am very grateful to my lab mates Dheeraj, Pradhyuman, Sagnik, Reeya, Raj, Maqsuma, Mukul, and Sahil for their pleasant company, cooperation, practical help and patronage. It was a great pleasure working with them and I appreciate their ideas, help and company throughout.

I am very exuberant to mention all my friends for always cherishing me at IISER Mohali. They are Divya, Gurjinder, Pratibha, Abhilasha, Suhasi, Saloni, Yashvi, Sakshi, Pooja, Pokhee, Navjot and many more whom I haven't acknowledged here for their direct or indirect help and motivation.

My joy knows no bounds in expressing my cordial gratitude to my dear parents whose love and support always encourages me to be at my best throughout my career. Last but not least, thanks to God for all the blessings he has bestowed on me and my family.

Abstract

In recent years, Pd-containing catalysts have emerged as alternatives to Pt due to Pd's strong catalytic activity, comparable characteristics, abundance, and affordable cost. Pd-based nanomaterials were applied as the binary compound catalyst for the excellent activity of oxygen reduction reaction (ORR) and alcohol oxidation reactions (EOR and MOR) for direct alcohol fuel cells (DAFC). This catalyst could inhibit particle agglomeration after a long processing time, require low production cost and exhibit good electro

In this study, Pd nanocomposite was prepared via the chemical reduction method. Powder X-ray diffraction (XRD) was applied to confirm the deposition of Pd on NrGO sheets. The solid-supported Pd catalysts were prepared on N-doped reduced graphene oxide (NrGO) sheets simply by the chemical reduction method. Sodium borohydride NaBH₄ was used as a reducing agent for the chemical reduction method. The uniform dispersion of Pd nanoparticles on N-doped reduced graphene oxide sheets, which were prepared by the chemical reduction method, was observed by transmission electron microscopy (TEM) techniques. TEM micrograph showed that particle sizes of synthesized catalysts were in the range of 3-4 nm.

The electrochemical performance of the catalyst was found to be suitable for both alcohol oxidation reactions (EOR, MOR) as well as for oxygen reduction reactions (ORR), so the designed catalyst can act as a potential bi-functional catalyst for Alcohol oxidation reaction (EOR, MOR) and Oxygen reduction reaction (ORR) in direct alcohol fuel cells (DAFCs).

List of Figures

Figure 1. Three different approaches to tailoring the physicochemical characteristics of NMNs are shown schematically, along with various new environmental applications that make advantage of these characteristics.

Figure 2. Comparison of d orbital energy levels of normal metals v/s d^8 metals.

Figure 3. Different forms of graphitic carbon.

Figure 4. Schematic illustrations of working principles for different energy storage devices: a) a fuel cell, b) a DMFC in acidic media, and c) a DMFC in alkaline media.

Figure 5. Advantages of Direct Alcohol Fuel Cells (DEFCs in particular).

Figure 6. Schematic diagram of the direct methanol fuel cell system.

Figure 7. Schematic diagram of the direct ethanol fuel cell system.

Figure 8. Schematic illustration of parallel pathways for Ethanol Oxidation Reaction.

Figure 9. Proposed mechanism of methanol oxidation via direct and indirect way.

Figure 10. Mechanism of Methanol oxidation reaction (MOR) in (a) acidic medium and (b) basic medium, respectively.

Figure 11. A simplified schematic pathway of oxygen reduction reaction for both acidic and alkaline media.

Figure 12. Schematic illustration for Oxygen reduction reaction (ORR) on surface of Nitrogen-doped carbon materials.

Figure 13. CHI760E electrochemical workstation for all electrochemical measurements.

Figure 14. Schematic illustration for the synthesis of Nitrogen-doped reduced graphene oxide (NrGO).

Figure 15. Nitrogen-doped reduced graphene oxide (NrGO) in Alumina boat.

Figure 16. Schematic of reduction of metal ions in solution.

Figure 17. Schematic representation of reaction setup for synthesis of metal nanoparticles composites on NrGO.

Figure 18. Microscopic characterization of NrGO : (a,b) TEM image at low resolution (c) high-resolution TEM image depicting (002) planes.

Figure 19. Microscopic characterization of Pd/NrGO (30% loading) : (a,b) TEM image at low resolution (c) the particle size distribution, (d) high-resolution TEM image, (e) corresponding SAED Pattern.

Figure 20. Microscopic characterization of Pd/NrGO (30% loading) with NaBH₄ addition at room temperature: (a,b) TEM image at low resolution (c) high-resolution TEM image, (d) corresponding SAED Pattern.

Figure 21. Pd/NrGO corresponding energy dispersive X-ray spectroscopic elemental mapping images.

Figure 22. Corresponding energy dispersive X-ray spectra for Pd/NrGO.

Figure 23. PXRD patterns of graphene oxide (GO), Nitrogen-doped reduced graphene oxide (NrGO) and Pd/NrGO (30% metal loading)

Figure 24. Schematic of Ethanol electrooxidation on Pd/NrGO surface.

Figure 25. Cyclic Voltammograms for electro-oxidation of ethanol using Pd/NrGO and Pd/C

Figure 26. Histograms showing mass activity for electro-oxidation of ethanol using Pd/NrGO and Pd/C.

Figure 27. Histograms showing specific activity for electro-oxidation of ethanol using Pd/NrGO and Pd/C.

Figure 28. Pd/NrGO and Pd/C MOR stability up to 100 cycles with a scan rate of 100 mV/s.

Figure 29. Pd/C EOR stability test for 500 cycles with a scan rate of 100 mV/s.

Figure 30. Pd/NrGO and Pd/C MOR stability up to 500 cycles with a scan rate of 100 mV/s.

Figure 31. The chronoamperometry curves for Pd/NrGO and Pd/C up to 3600 sec during ethanol oxidation reaction.

Figure 32. Schematic of Methanol electrooxidation on Pd/NrGO surface.

Figure 33. Cyclic Voltammograms for electro-oxidation of methanol using Pd/NrGO and Pd/C.

Figure 34. Histograms showing mass activities for methanol oxidation by Pd/NrGO and Pd/C.

Figure 35. Histograms showing specific activities for methanol oxidation by Pd/NrGO and Pd/C.

Figure 36. Pd/NrGO and Pd/C MOR stability up to 100 cycles with a scan rate of 100 mV/s.

Figure 37. Pd/NrGO and Pd/C MOR stability up to 500 cycles with a scan rate of 100 mV/sec.

Figure 38. The chronoamperometry curves for Pd/NrGO and Pd/C up to 3600 sec during methanol oxidation.

Figure 39. The ORR Polarization curves for Pd/NrGO (30% metal loading) in O₂ saturated 0.1 M KOH at different rotation rates of 400, 800, 1200, 1600, 2000 and 2400 rpm.

Figure 40. The ORR Polarization curves for Pd/NrGO (30% metal loading) and Pd/C in O₂ saturated 0.1 M KOH at the rotation rate of 1600 rpm.

Figure 41. The recorded cyclic voltammograms for ECSA determination of Pd/NrGO and Pd/C respectively.

Figure 42. Koutecky - Levich (K-L) plot for Pd/NrGO and Pd/C, respectively.

Figure 43. Histogram showing mass and specific activities for oxygen reduction reaction (ORR) by Pd/NrGO and Pd/C.

List of Tables

Table 1. Comparison of EOR performance of Pd-based nanostructures developed in this thesis with recently reported literature data.

Table 2. Comparison of MOR performance of Pd-based nanostructures developed in this thesis with recently reported literature data.

Abbreviations

M	Molarity
C	Celsius
NP	Nanoparticles
ECSA	Electrochemically Active Surface Area
Sec	Second
nm	Nanometer
g	Grams
mg	Milligrams
ug	Micrograms
A	Ampere
mA	Milliamperere
V	Volt
C	Coulomb
uC	Microcoulomb
ml	Milliliter
hrs	Hours
Pd	Palladium
rpm	Revolutions per minute
TEM	Transmission Electron Microscopy
PXRD	Powder X-ray Diffraction
SAED	Selected Area Electron Diffraction
EOR	Ethanol Oxidation Reaction
MOR	Methanol Oxidation Reaction
ORR	Oxygen Reduction Reaction

Contents

Abstract	VII
List of Figures	VIII
List of Tables	XII
1 Introduction	
1.1 Heterogeneous catalysts and nanomaterials for energy conversion	2
1.2 Noble metal-based nanomaterials	2
1.3 Nanotechnology in Energy Applications	4
1.4 Overview of Fuel Cells	6
1.5 Direct Alcohol Fuel Cells (DAFCs)	7
1.6 Advantages and Disadvantages of Direct Alcohol Fuel Cells (DAFCs)	8
1.7 Fundamentals of Direct Alcohol Fuel Cells (DAFCs)	10
1.8 Mechanism of Ethanol Oxidation Reaction (EOR)	12
1.9 Mechanism of Methanol Oxidation Reaction (MOR)	13
1.10 Mechanism of Oxygen Reduction Reaction (ORR)	15
1.11 Materials for Anode and Cathode in Direct Alcohol Fuel Cells (DAFCs)	18
1.11.1 Materials for Ethanol Oxidation Reaction (EOR)	19
1.11.2 Materials for Methanol Oxidation Reaction (MOR)	20
1.11.3 Materials for Oxygen Reduction Reaction (ORR)	21
2 Experimental Section	
2.1 Materials and Characterization	23
2.1.1 Chemicals Required	23
2.1.2 Characterization Techniques	23

2.2	Synthesis Method	24
2.2.1	Graphene Oxide synthesis by modified Hummer's Method	24
2.2.2	Synthesis of Nitrogen-doped reduced graphene oxide (NrGO)	24
2.2.3	Preparation of Pd/NrGO nanocomposite	24
2.3	Electrochemical Measurements	25
2.3.1	Preparation of Working electrode	26
2.3.2	Electrochemically Active Surface Area (ECSA)	26
2.3.3	Ethanol Oxidation Reaction (EOR)	27
2.3.4	Methanol Oxidation Reaction (MOR)	27
2.3.5	Oxygen Reduction Reaction (ORR)	28

3 Results and discussion

3.1	Synthesis of Palladium nanocomposite on Nitrogen-doped reduced Graphene oxide (NrGO) sheets	30
3.1.1	Synthesis of Support Material (NrGO)	30
3.1.2	Synthesis of Palladium nanocomposite supported on N-doped reduced graphene oxide sheets (Pd/NrGO)	30
3.1.3	Role of Support Material	33
3.1.4	Optimization of temperature of NaBH ₄ addition	35
3.1.5	Overview on optimum conditions for obtaining uniform distribution of nanoparticles on support material	35
3.2	Characterization of designed electrocatalyst (Pd loaded on NrGO)	36
3.2.1	Transmission Electron Microscopy-image Analysis	36
3.2.2	Energy Dispersive Spectroscopy	39
3.2.3	Powder X-ray diffraction (P-XRD) Analysis	40
3.3	Ethanol Oxidation Reaction (EOR)	41
3.3.1	Electrocatalytic EOR performance	42
3.3.2	Stability of the Catalyst Material	44
3.3.3	Comparison of EOR performance with literature reports	46

3.4	Methanol Oxidation Reaction (MOR)	47
3.4.1	Electrocatalytic MOR performance	48
3.4.2	Stability of the Catalyst Material	50
3.4.3	Comparison of MOR performance with literature reports	52
3.5	Oxygen Reduction Reaction (ORR)	53
3.5.1	Electrocatalytic ORR performance	53
4	Conclusion	56
5	Scope and future investigations	57
6	Reference	59

Chapter 1

Introduction

"Research is what I'm doing when I don't know what I'm doing" - Wernher von Braun

In the last few decades, humans have encountered two serious problems: environmental pollution and energy predicament due to the immense combustion of non-renewable fossil fuels and immediate emergent worldwide energy demands. The increase in the human population and the growing importance of technology have contributed to the upsurge in energy demand. Data from the US Energy Information Administration (EIA) have shown that energy utilization was roughly equal in 2007 between Organization for Economic Co-operation and Development (OECD) and non-OECD countries. However, from 2007 to 2035, OECD countries have been estimated to increase their energy use by 14%, while non-OECD countries are forecasted to grow by 84% ^[1]. Nowadays, energy applications in the form of electricity are predominant amongst electronic devices such as chargers for laptops, cameras, and mobile phones. These chargers or rechargeable batteries have the disadvantage of charging using an external electrical power source. This dependency is an obstacle to their usage due to an existing electrical source requirement, and the battery needs to be improved in capacity. Therefore, remote areas without any electric power source can encounter problems using devices operating on such batteries. Furthermore, the origins of electric power are mainly derived from fossil fuels, which harms the environment as the number of technology users depending on electricity continues to escalate. It was reported that nearly 6.2 billion tons of carbon dioxide were released into the atmosphere in 2000, and about 40% was due to emissions from electricity production.^[2] The increasing consumption of traditional fossil fuels and the severe environmental crisis has facilitated the rapid development of renewable and clean energy harvesting, conversion and storage technologies. Therefore, researchers have focused on developing clean energy technologies such as fuel cells as they have zero-emissions, hydrogen, oxygen, and methanol as fuel molecules and water as by-products. ^[3,4,5]

1.1 Heterogeneous catalyst and nanomaterials for energy conversion

In energy conversion-storage devices, active materials play a crucial role. Nanomaterials have enhanced the performance of many energy-harvesting devices due to their specific characteristic properties such as photovoltaics, piezoelectricity, ferroelectricity, and thermoelectricity. Developing efficient catalysts for redox reactions related to water splitting and carbon dioxide reduction reactions is the key to energy conversion devices. The materials used in these catalytic processes can be homogeneous or heterogeneous in nature. Homogeneous catalysts have disadvantages compared to heterogeneous catalysts in terms of stability and recyclability.^[6] Heterogeneous catalysts in the form of nanosized metal particles dispersed on microporous supports have been applied to energy conversion technologies for many decades. Heterogeneous catalysts promote reactions at the active sites on their surfaces, so they usually form nanoparticles with a large concentration of active surface sites. Thus, in order to access higher active surface area, synthesizing heterogeneous catalysts in the nanoscale is advantageous as they offer a much higher surface area. Confining the dimensions of material to the nanoscale also results in attractive physical and chemical properties of the materials, which leads to improved catalytic activities. The enormous advancements in modern nanotechnology are reflected in our expanded ability to design and control nanomaterials, their size, shape, chemical composition, and assembly structure for advanced applications.^[7] Controlling the shape, size and crystallinity of materials plays a crucial role since the efficiency of a catalyst has a strong dependence on the lattice packing of the catalyst's exposed surface. The use of surface stabilizers and capping agents are helpful in directing the shape and size of nanomaterials. Recent investigations on the developments of heterogeneous nano-catalysts have shown promising routes to improved device performances for energy conversion and commercialization of green fuel technologies.

1.2 Noble metal-based nanomaterials

Noble metal nanomaterials (NMN's) are functional materials with unique physical and chemical properties closely related to their size, shape, composition and structure.^[8] Significant progress has been made in the synthesis of novel noble metal nanocrystals and their potential applications in diverse fields such as in catalysis, electronics, and sensors.^{[9],[10]} Noble metals are

called noble because of their lower reactivity and resistance to corrosion and oxidation compared to other metals.^[11] Noble metals mainly comprise Ruthenium (Ru), Rhodium (Rh), Palladium (Pd), Silver (Ag), Gold (Au), Platinum (Pt), Osmium (Os) and Iridium (Ir). These metals with d^8 outer electronic configuration exhibit unique properties, which makes them catalytically more active because of less activation barrier of 0 and +2 oxidation states of metals due to the stability offered by d^8 and filled d^{10} orbitals. So, due to lower activation barriers and higher catalytic rate constants, noble metals frequently get a lot of attention from researchers because of their distinctive characteristics and potential for use in many different fields. The vast potential of using noble metal nanoparticles as agents for targeted drug delivery in living organisms, in photodynamic therapy of cancerous tumours, in the treatment of skin diseases, as biocidal disinfectants, as auxiliary material in the imaging of affected tissues, in catalysis, as well as in other areas is currently being actively investigated.^{[12],[13]}



Figure 1. Three different approaches to tailoring the physicochemical characteristics of NMNs are shown schematically, along with various new environmental applications that make advantage of these characteristics.^[10]

Noble metals being inert can remain in the metallic-state for much longer and act as catalysts for various reactions. Following are some possible explanations for superior catalytic activity of noble metals (specially, Pd and Pt) versus other metals ^{[14],[15]}:

1) Stability: A noble metal can be recognised by its resistance to oxidation or corrosion. Several low-valent, noble-metal complexes are stable enough to withstand a number of significant catalytic reactions under ambient settings without the strict requirement of an air-free environment, considerably enhancing their ease of operation.

2) Selectivity : Since they readily stand out with high activity and selectivity for numerous processes of both scientific and industrial importance, noble metals have been frequently exploited as heterogeneous catalysts.

3) Pi-bond affinity : Noble metals exhibits high affinity for pi-bonds which makes them suitable catalysts for various organic transformations and electrochemical reactions.

4) Characterization: Since noble metals are relatively stable, catalytically important noble - metal complexes may frequently be isolated and studied using a range of well used and established methods, such as nuclear magnetic resonance (NMR) spectroscopy and X-ray crystallography.

5) It is simpler for H_2/O_2 to dissociatively adsorb when the d- subshell is fully filled with electrons. So, noble metals can easily adsorb H_2/O_2 on their surface as compared to other transition metals.

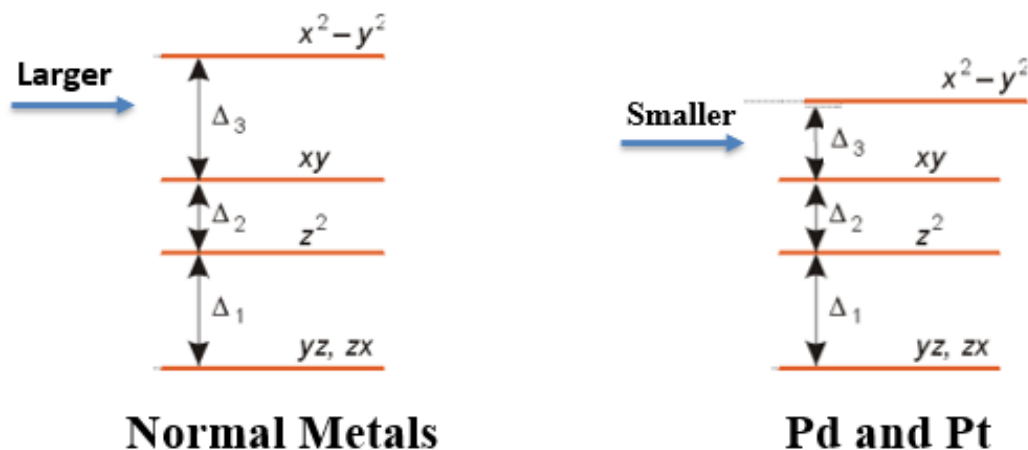


Figure 2. Comparison of d orbital energy levels of normal metals v/s d^8 metals

Ultimately, the predictable reactivity of noble-metal catalysts can be attributed to their electronic structure, which culminates in highly stable, uniquely selective, and easily characterized complexes as catalysts.

1.3 Nanotechnology in Energy Applications

At present developing efficient and “clean” energy technologies is an urgent task and is vital for the long- term energy and environmental security of our society.^[16] Due to classical and quantum scale effects on energy carriers including photons, phonons, electrons, and molecules, energy conversion and transport in nanomaterials differ significantly from that in bulk materials.

Batteries, fuel cells, and electrochemical capacitors are examples of systems for electrochemical energy conversion and storage. These three systems share "electrochemical commonalities" despite their differing energy storage and conversion processes. Similar characteristics include the energy-providing processes that separate ion and electron transport occur at the electrode/electrolyte interface's phase boundary. Fuel cells and batteries, such as polymeric electrolyte membrane fuel cells (PEMFC), solid oxide fuel cells (SOFC), and lithium-ion batteries, are electrochemical systems for conversion between chemical energy and electricity. They are made up of a cathode and an anode, which are separated by an electrolyte. Electrical energy is produced in batteries and fuel cells by converting chemical energy through redox processes occurring on the surface of the anode and cathode. The names "negative electrode" and "positive electrode" (denoted as "minus poles" and "plus poles," respectively) are used because reactions at the anode often occur at lower electrode potentials than at the cathode. Anode refers to the more negative electrode, whereas cathode refers to the more positive electrode. The difference between batteries and fuel cells is related to the locations of energy storage and conversion. Batteries are closed systems in which the anode and cathode serve as the charge-transfer medium and participate actively as "active masses" in the redox process. In other words, energy conversion and storage take place in the same space. Whereas, fuel cells are open systems where the anode and cathode are just charge-transfer media and the active masses undergoing the redox reaction are delivered from outside the cell. Thus, in a fuel cell energy storage and energy conversion are thus locally separated. The energy storage density of batteries and the efficiency of complete cells both can be considerably enhanced by the use of nanomaterials.^{[17],[18]}

The use of nanomaterials on the electrodes of electrochemical cells may enhance the charge storage capacity of batteries and the reaction rates of redox reactions in fuel cells. The ion conductivity of the electrolyte is one typical factor limiting the effectiveness of electrochemical systems. In the literature, it is shown that ionic transport can be dramatically

enhanced by using nanostructured composites. Nanostructured composites may have a very high charge storage capacity due to the nanoionics effect at heterogeneous interface between an insulating material with a high surface charge density and an ion conducting material. For example, nanomaterials such as carbon nanotubes, graphene, graphene oxide (GO), reduced graphene oxide (r GO), etc., provides high surface area to metal catalysts and acts as a good support material for metal nanocomposites.^[19] Figure below shows structure of graphitic carbon forms which are helpful in designing materials for energy conversion devices.

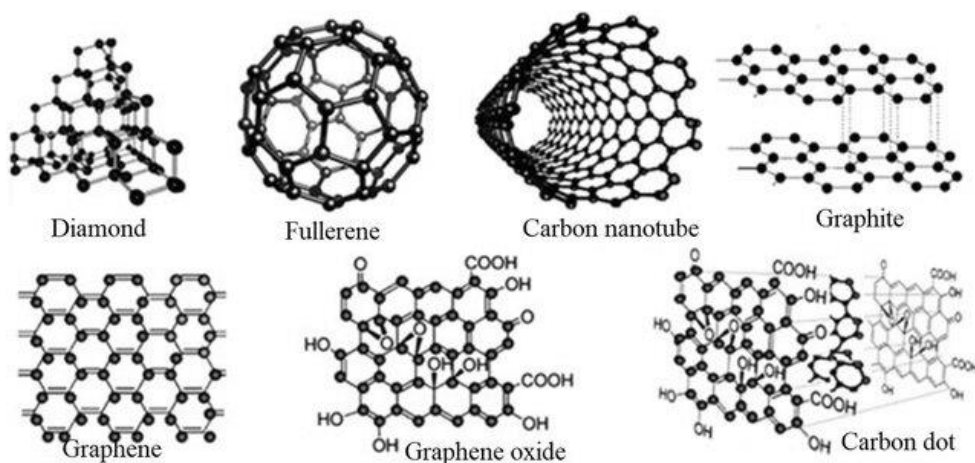


Figure 3. Different forms of graphitic carbon ^[20]

1.4 Overview of Fuel Cells

Among the novel energy conversion/storage devices, fuel cells are attracting much attention and have been considered very promising for mobile applications. Fuel cells are extensively employed in many fields, such as the generation of stationary and portable power as well as transportation. Fuel cells commonly possess combined merits, including simple structure, high energy density, fast rechargeability, easy to transport, and feasible fuel storage.^[21] Fuel cells are appropriate candidates for small to middle-sized power supplies with estimated power outputs ranging from several hundred watts up to 3 kW.^[22] These fuel cells generally utilize the concept of electrochemical reactions for energy conversion, which produces electricity from external supplies of anodic fuel and cathodic oxygen with the presence of electrolytes. The simplified structure of a fuel cell is shown in Figure 4 (a). A Typical fuel cell consists of two electrodes with an electrolyte membrane (EM) between them. During its function, the fuel/oxygen flows

into the fuel cell as reactants, and the reaction products subsequently flow out while the electrolyte remains.

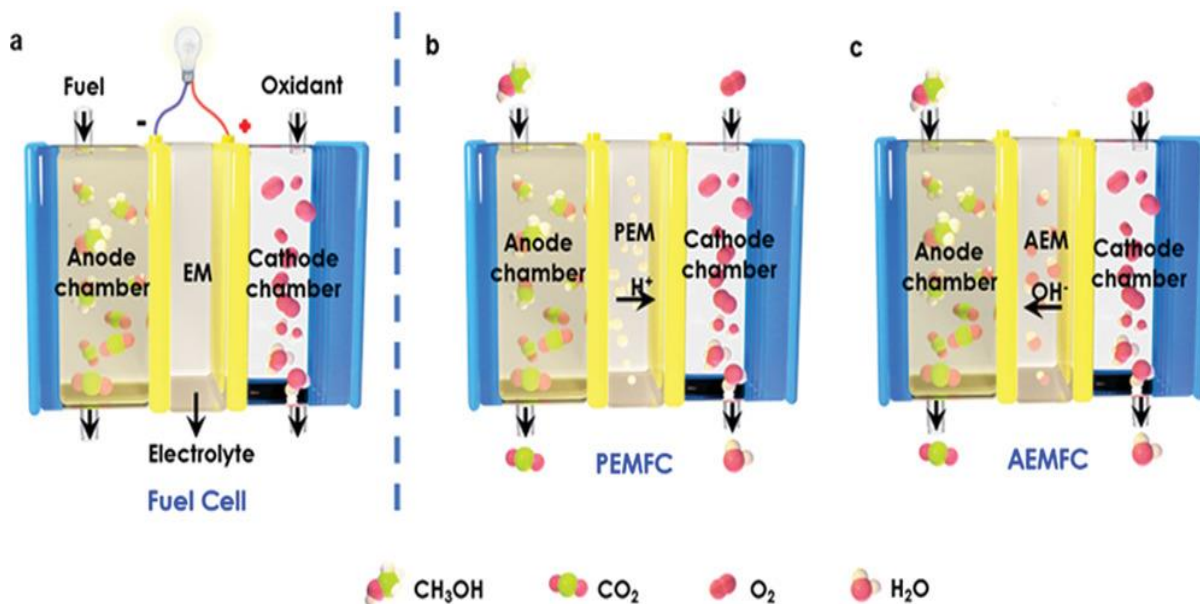


Figure 4. Schematic illustrations of working principles for different energy storage devices: a) a fuel cell, b) a DMFC in acidic media, and c) a DMFC in alkaline media.

Based on the differences in electrolytes and operating temperatures, fuel cells can be classified as direct alcohol fuel cells (DAFCs), proton exchange membrane fuel cells (PEMFCs, $\approx 80\text{ }^{\circ}\text{C}$), alkaline fuel cells (AFCs, $\approx 100\text{ }^{\circ}\text{C}$), phosphoric acid fuel cells (PAFCs, $\approx 200\text{ }^{\circ}\text{C}$), molten carbonate fuel cells (MCFCs, $\approx 650\text{ }^{\circ}\text{C}$), and solid oxide fuel cells (SOFCs, $\approx 650\text{--}1000\text{ }^{\circ}\text{C}$).^[23] Among the types of fuel cells, proton exchange membrane fuel cells (PEMFC), alkaline fuel cells (AFC), direct methanol fuel cells (DMFC), and phosphoric acid fuel cells (PAFC) are examples of the low-temperature fuel cell, while molten carbonate fuel cell (MCFC) and solid oxide fuel cells (SOFC) are examples of the high-temperature fuel cell. In low-temperature fuel cells, DAFC is one of the ideal energy sources of liquid fuel, low-cost, low-temperature requirement, high power density, quick refuelling, facile charging, and low environmental impact.^[24,25,26,27,28,29]

1.5 Direct Alcohol Fuel Cells (DAFCs)

Recently, the Direct Alcohol fuel cell (DAFC) has gathered enormous attention due to its unique qualities – high energy density, ease of liquid fuel storage, low cost, and low operating simplified system construction and minimal emission. Direct alcohol fuel cells (DMFC and DEFC) are a type of proton exchange fuel cell converting alcohols directly on the anode. The alcohol is fed directly into the fuel cell without any previous chemical modification and is oxidized at the anode while oxygen is reduced at the cathode. They attracted significant interest in the late 1990s for transport applications to overcome hydrogen infrastructure issues [30,31,32]. These systems are attractive for portable power sources because the design is relatively simple, the operating times are extensive, and the fuels are easily supplied from biomass.

Methanol is an attractive liquid fuel because it is relatively inexpensive, generally accessible, and easily stored and handled. Methanol has a specific energy of around 6 kWh/kg. Ideally, during the electrochemical oxidation of methanol six electrons are produced per methanol molecule which helps in production of electric current in the direct methanol fuel cell. However, methanol has some drawbacks; For instance, it is highly toxic and its by-product formaldehyde, if not oxidized completely, is also toxic. Due to these restrictions, scientists are looking into other alternative fuels.

Among the other alcohols, ethanol is a better alternative to methanol as a fuel for fuel cells. Ethanol is a renewable fuel and can be produced in large quantities from farm products and biomass. There is evidence that ethanol and its by-products are less toxic than other types of alcohol. Ethanol has a specific energy of around 8 kWh/kg. The complete electrochemical oxidation of ethanol to carbon dioxide and water can produce 12 electrons per ethanol molecule. Compared to methanol, ethanol has a higher boiling point (78°C) and is harmless. The issue with using ethanol as a fuel is that its C-C bond must be completely broken in order to be completely oxidised, which is challenging for modern electrocatalysts to do at temperatures below 100 °C. This frequently causes incomplete ethanol oxidation, which reduces fuel cell performance and may result in hazardous by-products or electrode deactivation. So, for commercialization of these devices, significant efforts have to be put on the development of systems with an optimum balance between cost, efficiency, and durability.^[33]

1.6 Advantages and disadvantages of Direct Alcohol Fuel Cells (DAFCs)

DAFCs have several benefits over their direct competitor, H₂-O₂ fuel cells. The main advantage of DAFCs is using liquid fuel, which makes handling and storage significantly easier. Especially for portable applications, primarily due to the lack of sufficient hydrogen storage technologies, the use of liquid fuel is the greatest alternative to obtain a high-power density with an appealing cost-to-power ratio. Some **advantages of Direct Alcohol fuel cells (DAFCs)** are namely:^{[34],[35]}

- 1) They have potential for high efficiency.
- 2) The design of DAFCs is very simple, with no moving parts, which makes DAFCs an excellent low-cost and highly durable choice for fuel cells.
- 3) DAFCs utilize alcohol molecules as fuel since alcohols like ethanol can be produced in large quantities from biomass through a fermentation process from renewable resources like sugar cane, wheat, or straw. Growing crops for biofuels absorbs a large portion of the carbon dioxide released into the environment from the fuel needed to manufacture the biofuels and from burning the biofuels themselves, making bio-generated ethanol (or bio-ethanol) appealing. Utilizing fossil fuels is in stark contrast to this. Ethanol usage would also solve hydrogen's infrastructure and storage problems of H₂-O₂ fuel cells.
- 4) In the case of fuel cells, there is no need for a recharge and power production remains continuous as long as fuel is supplied to the cell.
- 5) The issues of thermal management for small systems are reduced by the ability of DAFCs to function at ambient temperature.

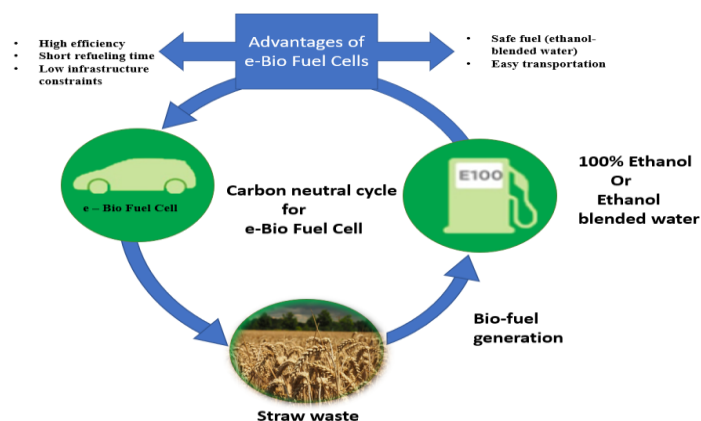


Figure 5. Advantages of Direct Alcohol Fuel Cells (DAFCs in particular)

Major problems in the commercialization of Direct Alcohol fuel cells (DAFCs) are:

- 1) The low temperature alcohol oxidation process is slow, which prohibits the DAFCs from having power densities that are on par with that of the H₂-O₂ PEM fuel cell.
- 2) Contaminants sensitivity is also a significant problem with DAFCs because these fuel cells require relatively pure fuel free of specific contaminants.
- 3) DAFC is facing many challenging technical issues related to its power systems' design, fabrication, and operation that remain unsolved. The high manufacturing cost of DAFC is one of the main drawbacks which hinders its successful commercialization. Mass transport of different species is another issue in DAFC which influences the system's performance, operating stability, and volumetric energy density.
- 4) The other key issues such as fuel supply, methanol crossover, durability and stability, and high cost also affects large scale commercialization of DAFCs.

1.7 Fundamentals of Direct Alcohol Fuel Cells (DAFCs)

Several under-developed fuel cell types are currently available, including direct and indirect alcohol fuel cells, oxygen-ion proton conducting electrolytes, and solid/liquid electrolyte-based systems. In indirect alcohol fuel cells, alcohol is first transformed into H₂ and CO, which may then be used as fuels in high-temperature fuel cells like solid oxide or molten carbonate. In contrast, in low-temperature fuel cells like proton exchange membrane fuel cells, CO is transformed into H₂ and CO₂. Other alcoholic fuels used in fuel cells besides ethanol are methanol (CH₃OH) and ethylene glycol (CH₂OH)₂. The complete oxidation of hydrogen, methanol, ethanol, and ethylene glycol requires 2, 6, 12, and 10 electrons, respectively.^[36]

Direct Methanol Fuel Cells (DMFC) and Direct Alcohol Fuel Cells (DEFC) are the two main direct alcohol fuel cells (Direct Ethanol Fuel Cell).

a) Direct Methanol Fuel cell (DMFCs)

In the direct methanol fuel cells, firstly oxidation of methanol takes place at the anode which in turn produces six electrons and protons and then protons cross the membrane and reach cathode for carrying out oxygen reduction reaction and six electrons generated in methanol complete oxidation thus helps in the generation of electricity through DMFCs.

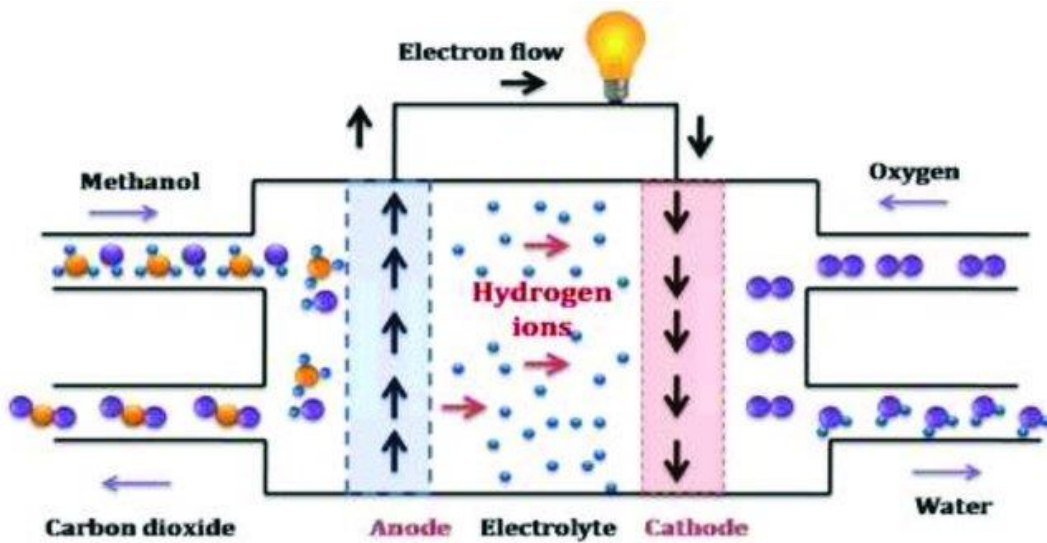


Figure 6. Schematic diagram of the direct methanol fuel cell system^[37]

b) Direct Ethanol Fuel cell (DEFCs):

In the direct ethanol fuel cells firstly oxidation of ethanol takes place at the anode which in turn produces twelve electrons and protons and then protons cross the membrane and reach cathode for carrying out oxygen reduction reaction and electrons generated in ethanol complete oxidation thus helps in the generation of electricity through DEFCs.

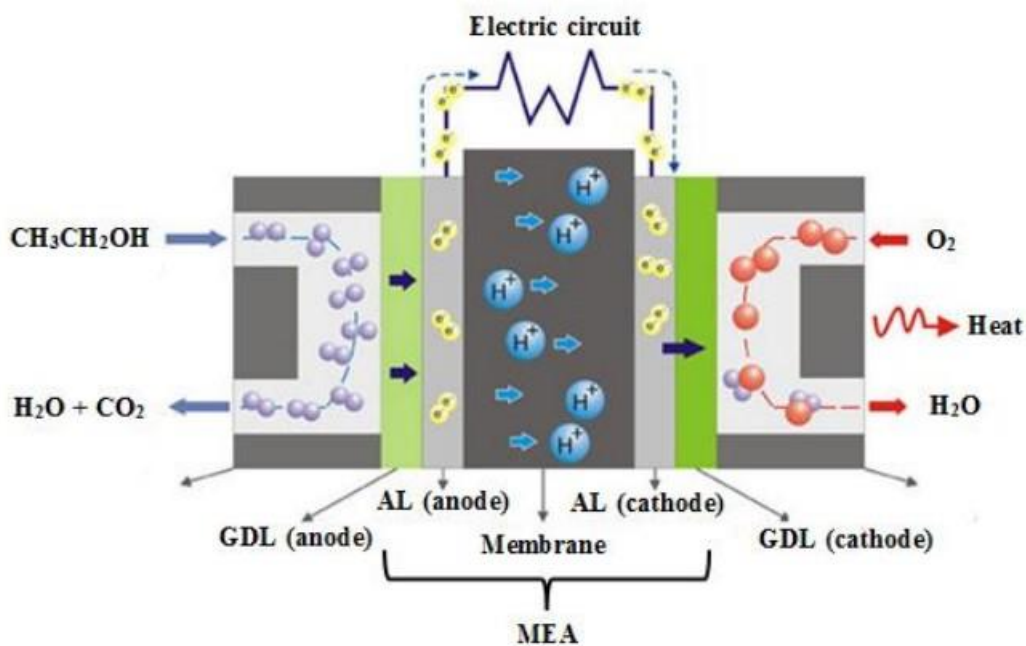


Figure 7. Schematic diagram of the direct ethanol fuel cell system^[38]

1.8 Mechanism of Ethanol Oxidation Reaction (EOR)

The EOR (Ethanol Oxidation Reaction) has a complex mechanism which can follow different reaction pathways. The primary EOR pathway, also known as the complete ethanol oxidation process, produces CO₂ as the reaction's by-product and generates 12 electrons. Obviously, this reaction, which can produce up to 12 electrons, cannot occur in only one step. Instead, it is an electrochemical reaction that is kinetically sluggish and separated into a series of elemental reactions in which each of these elementary reactions has the involvement of a distinct reaction intermediate.^{[39],[40]}

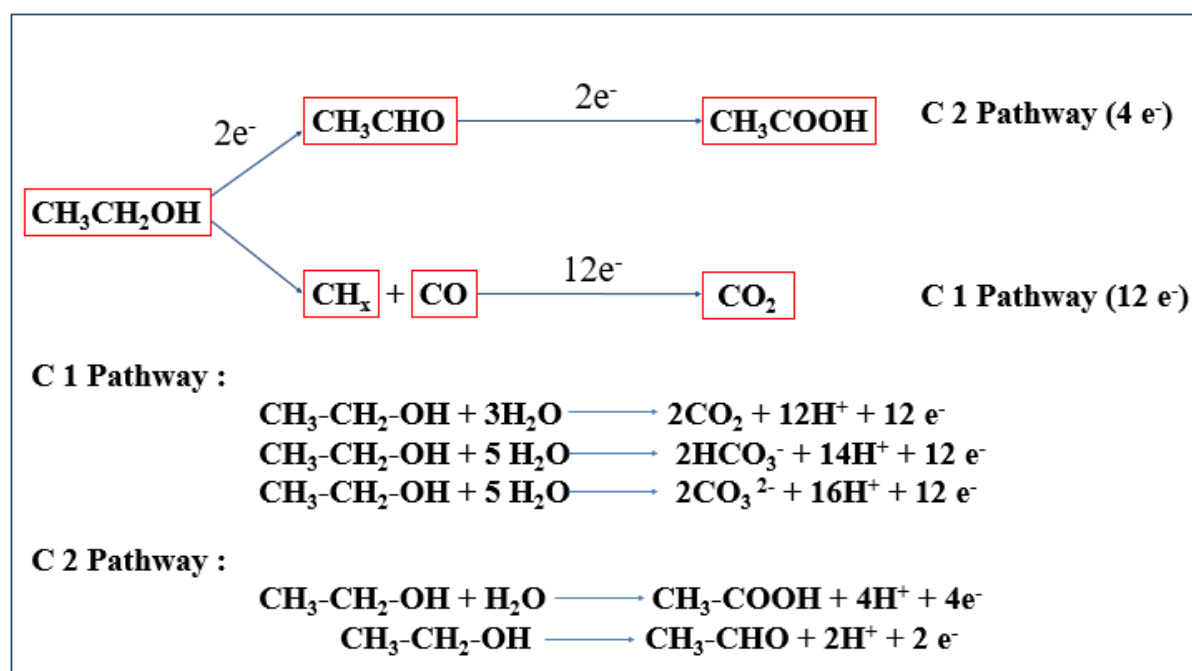


Figure 8. Schematic illustration of parallel pathways for Ethanol Oxidation Reaction

The C 1 pathway is the total oxidation of ethanol to CO₂ or carbonates through CO_{ads} intermediate by delivering 12 electrons, whereas, the C 2 pathway is the partial oxidation of ethanol to acetate by supplying four electrons or to acetaldehyde by delivering two electrons without the breaking of the C–C bond as shown in the figure 8 above.

The mechanism of Pt- or Pd-based catalysts have been extensively studied in an effort to know more about the intermediates and products of EOR. Figure 8 illustrates the commonly accepted

dual-pathway mechanism of EOR on Pt- or Pd-based catalysts in either acidic or alkaline conditions.^[41]

1.9 Mechanism of Methanol Oxidation Reaction (MOR)

The methanol oxidation reaction is a process which involves the transfer of six electrons.

Methanol is the most promising molecule due to its high energy density and its full oxidation to carbon dioxide. The thermodynamic potential for methanol oxidation reaction (MOR) is 0.02 V.

During electrochemical methanol oxidation reaction different products can form depending on reaction conditions like pH etc., and the overall reaction pathway can be described in these three steps such as:

1. Stepwise dehydrogenation of methanol to CO_{ads} and subsequent oxidation of CO_{ads} to CO_2 ;
2. Reaction along parallel, “direct” paths to CO_2 ;
3. Partial oxidation to formic acid and/or formaldehyde

The overall reaction pathway is shown in Figure below :

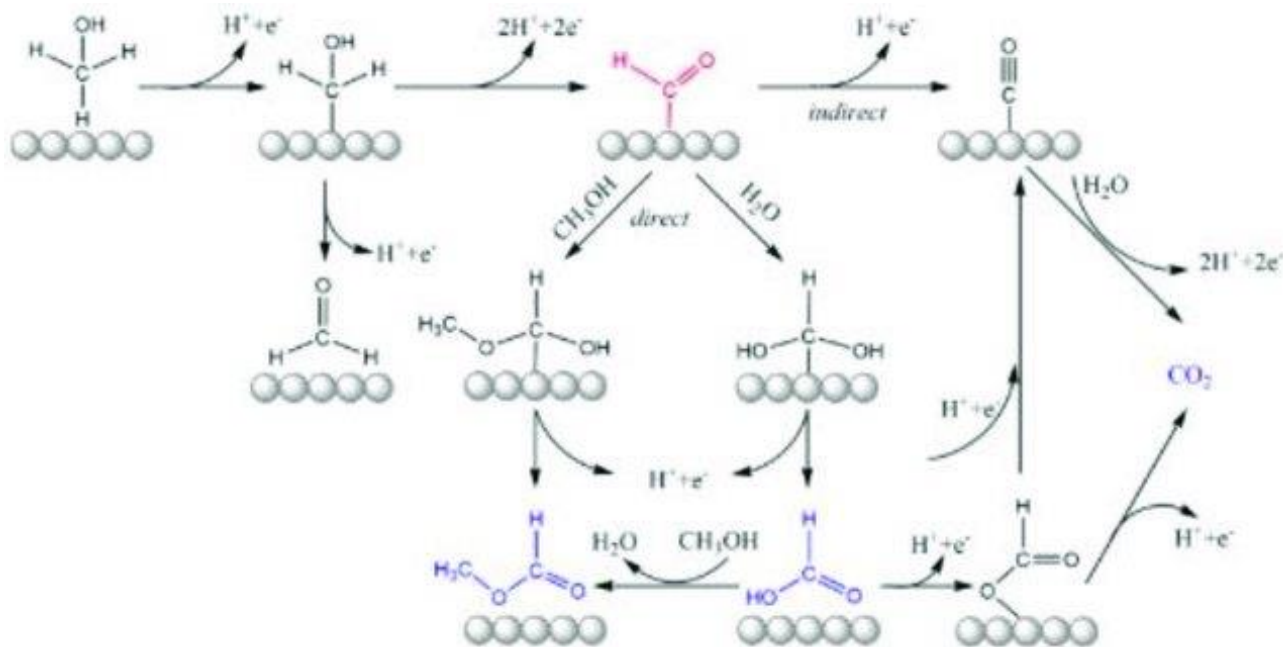
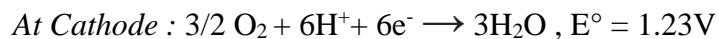
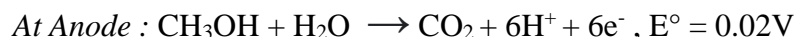


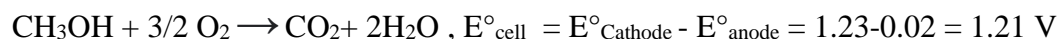
Figure 9. Proposed mechanism of methanol oxidation via direct and indirect way ^[42]

The methanol oxidation can be carried out in both acidic and basic media. The MOR process in acidic and basic media can be represented as follows:^[43]

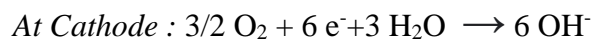
- **In Acidic Medium:**



Overall, Cell Reaction:



- **In Alkaline Medium:**



Overall, Cell Reaction:



In an alkaline medium, the hydroxide ions present in the electrolytic solution get adsorbed on the surface of the electrode and lead to the formation of hydroxide or oxide on the surface of the electrode.

The detailed reaction mechanism in the alkaline medium on Palladium surface can be expressed as follows:



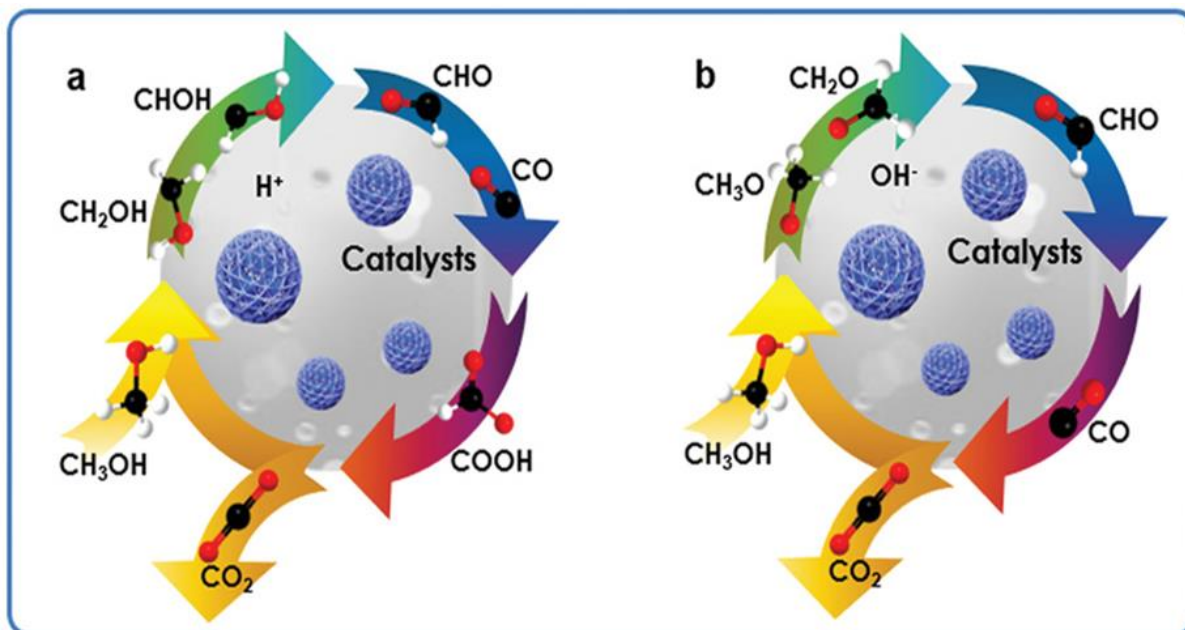


Figure 10. Mechanism of Methanol oxidation reaction (MOR) in (a) acidic medium and (b) basic medium, respectively ^[44]

1.10 Mechanism of Oxygen Reduction Reaction (ORR)

Oxygen reduction reaction is a cathodic reaction in Direct alcohol fuel cell (DAFCs). ORR is considered as the bottleneck for the efficient functioning of fuel cells because of its sluggish reaction kinetics compared to hydrogen oxidation reaction (HOR).

Oxygen Reduction Reaction (ORR) is a chemical reaction that involves the reduction of oxygen molecules O_2 to water H_2O or hydroxide ions (OH^-) in an electrochemical cell. The ORR is a critical process in many important technologies, including fuel cells, batteries, and metal-air batteries.

In a fuel cell, ORR is the process of converting oxygen and hydrogen fuel into water and electrical energy. In a battery, ORR is the process of recharging the battery by reversing the discharge reaction. In both cases, the ORR is a complex electrochemical process that involves the transfer of electrons and ions between the electrode and the electrolyte.

The ORR is typically performed using a catalyst, which is a substance that speeds up the reaction without being consumed in the process. Platinum (Pt) is the most common catalyst

used for ORR, but it is expensive and limited in supply. Therefore, researchers are actively searching for alternative catalysts that are cheaper and more abundant, such as iron-based catalysts and Palladium based catalysts.^[45]

The mechanism of oxygen reduction reaction (ORR) can be complex, depending on the specific conditions of the reaction and the type of catalyst used. The exact mechanism and reaction intermediates can depend on the specific catalyst used, as well as the pH, temperature, and other conditions of the reaction. For example, in acidic conditions, the intermediates may be different than in alkaline conditions, and the reaction may proceed through different pathways. Overall, the ORR is a complex electrochemical process that involves the transfer of electrons and ions between the catalyst, electrode, and electrolyte.

However, in aqueous medium ORR mainly occurs via two pathways:^[46]

- i. Direct 4 electron reduction of O₂ to H₂O
- ii. 2 electron reduction of O₂ to H₂O

The ORR reaction mechanism in acidic and alkaline medium can be expressed as follows:

In Acidic medium,



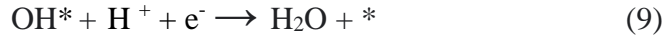
In Alkaline medium,



Among above chemical reactions equation (1) and (4) represents direct 4 e⁻ reduction process which is preferred for fuel cell applications whereas 2e⁻ processes are important for industrial production of H₂O₂ (hydrogen peroxide). The thermodynamic potential for 4 e⁻ ORR process is 1.23 V (vs NHE).

The direct 4 electron reduction of O₂ to H₂O can occur by two mechanisms as follows:

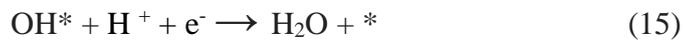
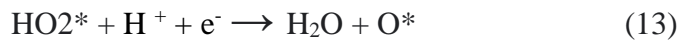
1) Dissociative Mechanism:



On the catalyst surface, O₂ first adsorbed on the catalyst surface and then it splits to atomic oxygen (eq.7), and then this atomic oxygen got reduced to H₂O by 2e⁻s in two consecutive steps (eq. 8 & 9).

Since the catalyst surface is not able to stabilize O₂, therefore H₂O₂ cannot be formed by dissociative mechanism.

2) Associative mechanism:



Associative mechanism does not involve H₂O₂ as intermediate. However, if the O-O bond in the adsorbed species (in eq. 11) is not broken, then it may result in the formation of H₂O₂ and then this H₂O₂ can be further reduced to H₂O or can be desorbed as final product.

In both dissociative and associative mechanism of ORR * represents active sites on the catalyst surface.

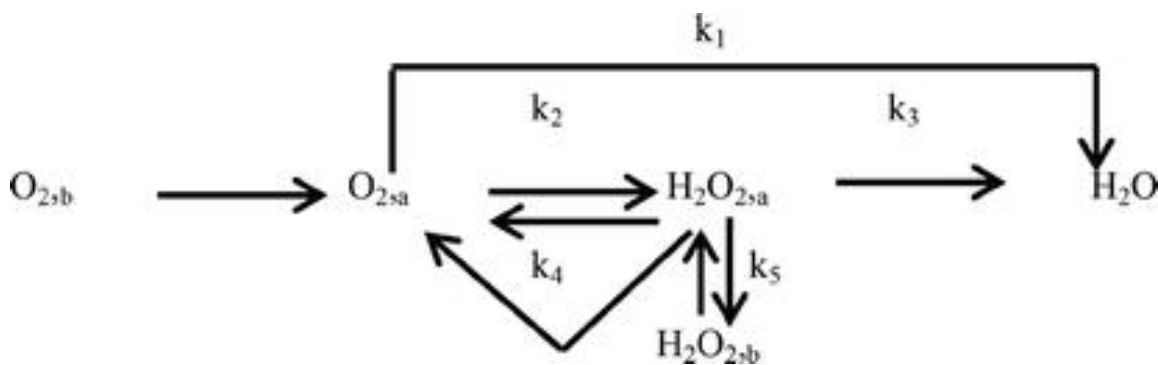


Figure 11. A simplified schematic pathway of oxygen reduction reaction for both acidic and alkaline media^[47]

1.11 Materials for Anode and Cathode in DAFCs :

In direct Alcohol fuel cells (DAFCs) at anode alcohol oxidation reaction takes place and at cathode oxygen reduction reaction takes place. Both the cathode and anode reaction efficiencies are highly dependent on the surface structure of the catalyst, which in turn determines the fuel cell's total efficiency. But, the major challenge in the commercialization of fuel cell technology is related to the high cost of platinum though its electronic structure makes it a promising catalyst for both cathode reaction as well as anode reaction. Pd acts as a promising alternative for Pt due to its similarities with Pt and for being inexpensive and comparatively more abundant. In addition, a few fundamental properties have still to be considered in the quest for Pd-based catalysts with superior electrocatalytic performance compared to Pt-based catalysts. Some of them are:

i. Controlling the exposed facets:

Electrocatalytic performance for both ORR and MOR were predicted to be strong for Pd catalysts with the (100) exposed facet. Thus, Pd nanostructures with exposed (100) facet should be prepared with better yield.

ii. Tailoring d- band centre position:

Pd's strong binding with oxygen and oxygenated intermediates lowers ORR performance. Hence, oxygen binding strength may be adjusted by shifting the centre location of the d-band by removing electron density from the surface of Pd. Many methods, including alloy production and the generation of metal-support interaction, are explored in this thesis in an effort to fine-tune the location of the Pd d-band centre.

iii. Creating self-supported nanostructures:

After being loaded onto a support material, a Pd nanocrystal loses between 25-50 % of its geometric surface area because some of its active sites are now hidden beneath the surface of the support. Therefore, Pd's efficiency in both alcohol oxidation reactions (MOR, EOR) and oxygen reduction reactions can be maximised by fabricating a self-supported nanostructure of Pd, such as a nanocrystal superlattice or nanoparticles deposited on some support materials like graphene oxide, reduced graphene oxide, or nitrogen doped reduced graphene oxide (ORR).

iv. Improving stability:

Incorporation of a non-noble metal into Pd lattice can increase the durability of nanostructures by making Pd more resistant to oxidation.

The efficiency of Pd-based catalysts can be improved by following these approaches though these have yet to be broadly investigated, thus, needing further research efforts.

1.11.1 Materials for Ethanol Oxidation Reaction (EOR)

Popular catalysts for ethanol oxidation reaction (EOR) include those based on platinum and palladium, which perform optimally in acidic and alkaline conditions, respectively. However, when put through prolonged term cycle testing, pure Pt and Pd typically show insufficient C-C bond cleavage capacity and unstable catalytic performance.^[48] In addition to the noble metal's prohibitively high price, these issues are the primary roadblocks to widespread Pt and Pd use in industry. Therefore, significant efforts have been directed to design highly active and stable catalysts for EOR, such as the formation of composite catalysts, optimization of support materials, composition and morphology control.

Since the microstructure of catalysts plays a significant role in the EOR process, optimising their shape and size is crucial for improving their catalytic efficacy in EOR. To improve the reaction kinetics of Pt and Pd catalysts, morphology control via nanostructure engineering has been frequently used to increase surface areas or expose particular facets. These nanostructured Pt or Pd based catalysts for EOR have shown promising results, but their stability is still an

issue ^[49]. Because of this, Pt- and Pd-based alloys have been produced with the addition of non-precious elements. Pt-based catalysts usually exhibit higher EOR activity in an acidic medium, whereas those based on Pd may effectively oxidise ethanol in alkaline environments. In addition, Pd's oxyphilic nature makes it easier for intermediate by-products to undergo oxidative desorption, which can reduce the poisoning impact on the catalyst. Pd-based catalysts have these characteristics, making them a viable choice for increasing EOR activity in alkaline electrolytes.^[50]

For example, in a recent study, Li et al. reported the use of Ni(OH)₂ to improve the catalytic activity of Pd nanoparticles in the EOR. They prepared a hybrid electrocatalyst composed of Pd nanoparticles, defective Ni (OH)₂ nanoflakes, and a graphene support through a two-step solution method ^[51]. Integrating noble metals (like Pd and Pt) with other transition metals and their deposition on some support materials in a rational design capable of oxidising alcohol molecules at the anode is expected to reduce the overall cost of DAFCs.

1.11.2 Materials for Methanol Oxidation Reaction (MOR)

There has been a great deal of research undertaken to find a cheaper alternative to the pricy Pt/C used in fuel cell applications for electrocatalytic MOR. As an alternative to Pt, Pd has been utilised as an electrocatalyst for the oxidation of small molecules, including methanol. Moreover, Pd is more resistant to CO poisoning than Pt because surface hydroxides develop more readily on Pd's surface than Pt's, aiding in the subsequent oxidation of CO to CO₂.

Due to its large surface area and abundance of electroactive centres, palladium nanostructures (a noble metal) have grabbed the interest of scientists studying several electrocatalytic processes. The long-term stability, large surface area, and porous nature of these nanostructures make them ideal for improving a variety of electrochemical processes.

Nanowires, nanoflowers, nanoplate arrays, nanoparticles, and nano-trees are only few of the palladium structures that have been synthesised in the past and shown to exhibit remarkable electrocatalytic activity in oxidation processes involving ethanol and methanol. The use of conductive support in composites also boosts their efficiency. For example, the oxidation of formic acid and methanol can be aided by combining palladium nanoparticles with nitrogen and doped graphene. Pd/NS-G has the highest mass specificity and current density than Pd/undoped graphene and Pd/Vulcan XC-72 R catalysts, which may be the result of improvements in

palladium efficiency. Pd-NPs/PVP-graphene, Pd/TiO₂-C, Pd/CNF, etc. are some of the other Pd-based MOR catalysts being investigated.^[52,53,54,55]

Strong interactions between metal and support material leads to charge transfer between active phases and the support in noble metal nanoparticles supported nanocomposites, and this one-of-a-kind structural property optimises OH⁻ and CO adsorption energy on the surface of the catalyst, leading to superior electrocatalytic performance.

It has been observed that the synergistic effect between the oxides, hydroxides and noble metal particles plays a crucial role in enhancing the activity and stability of the hybrid material for MOR.

1.11.3 Materials for Oxygen Reduction Reaction (ORR)

Pt is considered the most effective catalyst for oxygen reduction reaction (ORR) ; its oxygen reduction efficiency decreases in alkaline media compared to the acidic medium. Because of their shared atomic size and crystal structure in the periodic table, Pt and Pd have many of the same characteristics. Due to their superior catalytic activity in alkaline medium, nanostructures based on palladium have gained a lot of interest as cathode catalysts. Recent studies have focused on improving the intrinsic catalytic activity of Pd-based nano catalysts using various means, such as alloying, shrinking the size of the nanocrystals, modifying the surface, regulating the shape and composition, creating metal-support interactions, etc. It was found that carbon-based materials had been seen as the most promising replacement for expensive and limited Pt-based catalysts (ORR) for the oxygen reduction process. It was found that Carbon-based materials had been seen as the most promising replacement for expensive and limited Pt-based catalysts (ORR) for the oxygen reduction process. Because the surface of carbon is chemically inert, activating it is a prerequisite for oxygen reduction reaction (ORR). Doping with heteroatoms has been studied since it is thought to be an efficient activation strategy. The strong electronic affinity of the N atom is thought to disrupt the electrical neutrality of the carbon matrix, resulting in a high positive charge density in the adjacent carbon atoms. These positively charged carbon atoms have the potential to serve as chemisorption sites for O₂, leading to an efficient reduction of the O₂ molecule to H₂O via a 4e⁻ process. Nakamura and co-workers constructed a series of model catalysts with well-controlled doping of N species to investigate the effect of each type of N on ORR activity. They experimentally found that the

carbon atoms with Lewis basicity next to pyridinic N rather than that next to graphitic N are the actual ORR active sites in N-doped carbon materials, suggesting that pyridinic N is more important to ORR activity than graphitic N.^[56]

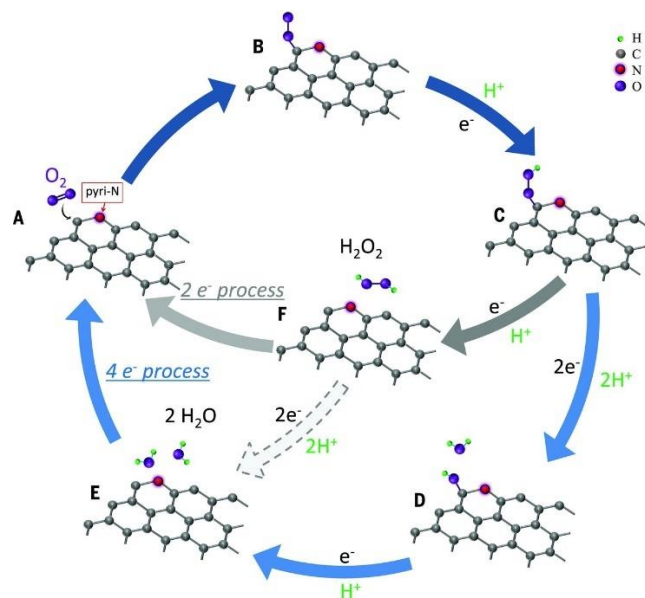


Figure 12. Schematic illustration for Oxygen reduction reaction (ORR) on surface of Nitrogen-doped carbon materials.^[56]

Zhang et al. synthesised ultrafine Pd Co bimetallic nanoparticles encapsulated in N-doped porous carbon nano capsules (PdCo@NPNCs), demonstrating enhanced ORR activity than commercial ones Pt/C in alkaline media. The N-doped porous carbon shell could effectively inhibit agglomeration, detachment, and dissolution of NPs during fuel cell operation. High surface area and superior electrical conductivity have made carbon-based materials like carbon black, graphene, carbon nanotubes, etc., attractive support materials.^[57]

Chapter 2

Experimental Section

2.1 Materials and Characterization Techniques

2.1.1 Chemicals Required

Ruthenium Chloride (RuCl_3), Palladium chloride (PdCl_2 , 99%, Alfa Aesar), Graphite powder (Alfa Aesar), KMnO_4 (Rankem), H_2SO_4 (Himedia), H_3PO_4 (Himedia), HCl (Himedia), H_2O_2 (Rankem), conc. HCl (Himedia, 35%), Pt/C (20 wt% Pt on carbon support, Sigma-Aldrich), Pd/C (30 wt% Pd on carbon support, Sigma-Aldrich), NaBH_4 (99%, Sigma Aldrich), melamine (Sigma Aldrich), potassium hydroxide (KOH, Himedia), Methanol (CH_3OH , Himedia), Nafion (5% in aliphatic alcohol, Sigma Aldrich), potassium hydroxide (KOH, Himedia), Methanol (CH_3OH , Himedia, molecular biology grade). All the chemicals were used without further purification. All the experiments were performed in ultrapure water with resistivity of 18.2 $\text{M}\Omega$.

2.1.2 Characterization Techniques

Transmission electron microscope (TEM) and high-resolution TEM (HRTEM) images were taken using JEOL JEM-F200 equipped with electron energy loss spectroscopy (EELS) and energy-dispersive X-ray spectroscopy (EDS, Bruker Instruments). The TEM was operated at 200 kV. TEM grids were plasma cleaned using Solarus plasma cleaner (Gatan) for 30 second before use. TEM samples were prepared by drop casting an ethanol dispersion of catalyst material on a holey carbon-coated Cu grid and allowing it to dry in air at room temperature for an hour followed by vacuum drying.

Powder X-ray diffraction (XRD) patterns were collected using a Rigaku Ultima IV diffractometer with Cu K X-ray radiation (generator power setting: 40 mA and 40 kV)

equipped with a DTex Ultra detector using parallel beam geometry at a scanning rate of $2^{\circ} \text{ min}^{-1}$ and scan step of 0.02° for the 2θ range of $5-80^{\circ}$. The samples were grounded to make fine powder using a mortar and pestle prior to the measurement.

2.2 Synthesis Method

2.2.1 Graphene Oxide synthesis by modified Hummer's Method

In the typical synthesis procedure, firstly, graphene oxide (GO) was produced using the modified hummers method from pure graphite powder. In this method, 120 ml of sulfuric acid (H_2SO_4) and 13 ml of phosphoric acid (H_3PO_4) (volume ratio 9:1) were mixed and stirred for several minutes. Then, this 133 ml of an acidic mixture was slowly added to a beaker containing 1 g of commercially available graphite powder and 6 g of KMnO_4 and placed on an ice bath to maintain the solution temperature below 10°C . After that, the reactant mixture was heated at 55°C for 12 h with constant stirring. Then the reaction mixture was cooled to room temperature by adding 130 g of ice. After that, 1.5 ml of H_2O_2 (30%) was added to the reaction mixture, which immediately changed the solution's colour to yellow, indicating the formation of graphene oxide (GO).^[58]

2.2.2 Synthesis of Nitrogen-doped reduced graphene oxide (NrGO)

For the synthesis of Nitrogen doped reduced graphene oxide (NrGO), 1.2 g of GO and 6 g of melamine ($\text{C}_3\text{H}_6\text{N}_6$) were dispersed in 100 ml and 400 ml of water, respectively, under sonication. Melamine suspension was then added to GO dispersion and kept under vigorous magnetic stirring at room temperature for 12 h to form a homogenous solution. Then the solution temperature was raised to 55°C to evaporate the water. The dried sample was well grounded using a mortar pestle and pyrolyzed inside a tube furnace under an Ar atmosphere (with a heating rate of $5^{\circ} \text{C min}^{-1}$) at 350°C for 3 h and subsequently at 1000°C for 30 min to get NrGO from NGO. Finally, the furnace was naturally cooled to room temperature, and the product was collected.

2.2.3 Preparation of Pd/NrGO nanocomposites

The noble-metal nanoparticle composite was synthesised at room temperature using water as a solvent by simple chemical reduction method with NaBH₄ as a reducing agent. The specific experimental procedure is as follows: 15 mg of NRGO was first dispersed in 10 ml of water by keeping under vigorous magnetic stirring for 2 hrs. Then 5 ml, 0.15 mmol Metal precursor solution (K₂PdCl₄ for Pd) was prepared using water and 2M HCl. The metal pre-cursor solution was then added dropwise to the NrGO dispersion, and the resulting mixture was stirred for 2.5 hrs. at 1000 rpm. 4 ml, 0.5M NaBH₄ solution was then slowly added to the reaction mixture under ice-cold conditions. Finally, the reaction mixture was stirred at 1000 rpm for 12 hr overnight. The product was collected by centrifugation at 13500 rpm and further washed several times with double distilled water and absolute ethanol. It was dried in vacuum oven at 60°C and further used for characterization and catalysis. Another set of Pd/NrGO catalyst was synthesised by following the similar procedure as above with the addition of reducing agent (NaBH₄) at room temperature in order to see the effect of NaBH₄ addition on nanoparticles size and distribution on the surface of support material (i.e., NrGO).

2.3 Electrochemical Measurements

The electrocatalytic performances were measured using a GC-RDE and RRDE connected to CHI760E electrochemical workstation. A conventional three-electrode setup was used with a reference electrode, Hg/Hg O (0.1 M NaOH) for alkaline media, Hg/Hg₂SO₄ (0.5 M H₂SO₄) for acidic media and Ag/AgCl (3M K Cl) for neutral media. Pt wire or graphite rods were used as a counter electrode. For comparison, all potential values were converted and plotted with respect to reversible hydrogen electrode (RHE) using following equation:^[59]

$$E_{\text{RHE}} = E_{\text{observed}} + 0.0591 \times \text{pH} + E^{\circ}_{\text{reference}}$$

where,

E_{observed} = experimentally observed potential using Hg/HgO reference electrode

$$E^{\circ}_{\text{Hg/HgO}}(0.1\text{MNaOH})=0.165\text{V}$$

$$E^{\circ}_{\text{Hg/Hg}_2\text{SO}_4}(0.5\text{MH}_2\text{SO}_4)=0.68\text{V}$$

$$E^{\circ}_{\text{Ag/AgCl}}(3\text{M K Cl}) = 0.21\text{ V}$$

The whole experimental setup and three electrode setup is shown in Figure below:



Figure 13. CHI760E electrochemical workstation for all electrochemical measurements.

2.3.1 Preparation of Working Electrode

Before use, firstly, the GCE, GC-RDE electrode was well polished with 0.05-micron alumina powder and cleaned by ultrasonication in water and isopropyl alcohol to get a mirror finish surface. Catalyst ink for the working electrode was prepared by dispersing the de-sired amount of catalyst in the required amount of Nafion:isopropanol:water (in the ratio of 0.5:1:4) solution by ultrasonication for 20 minutes. The working electrode was prepared by drop-casting the desired amount of catalyst ink on to pre-cleaned glassy carbon (GC) rotating disk electrode (RDE) with a geometric surface area of 0.0707 cm^2 and dried overnight at ambient conditions. The total metal loading on GC was estimated to be 0.2 mg/cm^2 on the electrode surface. Similarly, the metal loadings commercial Pt/C and Pd/C were maintained to be 0.2 mg/cm^2 on the electrode surface on the electrode surface.

2.3.2 Electrochemically Active Surface Area (ECSA)

For ECSA determination, the cyclic voltammograms (CVs) were recorded in Ar saturated 1 M KOH and the potential was scanned from 0.04 to 1.2 V (vs. RHE) at a scan rate of 50

mV s⁻¹. The scan was repeated several times to ensure that a stable CV was obtained. The ECSA was estimated using the following formula:

$$\text{ECSA} = Q_{\text{Pd}} / (\Gamma) \text{ (Pd in mg)}$$

,where, Q = is the charge accumulated for reduction of Pd (OH)₂ calculated from the CV, Γ = is the charge deposited per unit surface area of the electrode for the formation of Pd(OH)₂ (405 $\mu\text{C}/\text{cm}^2$).

2.3.3 Ethanol Oxidation Reaction (EOR)

The electrocatalytic activity of Pd/NrGO sheets, commercial 30% Pd/C, and commercial 40% Pt/C towards MOR was studied by Cyclic Voltammetry (CV) technique. The CV measurements for MOR were obtained in N₂-saturated 1 M CH₃CH₂OH + 1 M KOH solution, and the potential was scanned from 0.3 to 1.5 V (vs RHE) at a scan rate of 50 mV s⁻¹. The scan was repeated several times to ensure that a stable CV was obtained. The stability of electrocatalyst was evaluated by chronoamperometry at a potential corresponding to the forward peak current for 3600 s in a freshly made electrolyte solution containing 1 M CH₃CH₂OH and saturated with N₂.

Mass activity ($I_{k, \text{mass}}$) of the designed catalyst can be calculated by dividing forward peak current for ethanol oxidation with mass loading of noble metal (Pd or Pt).

$$\text{Mass Activity} = \text{Forward peak Current} / \text{Noble metal loading}$$

Specific Activity ($I_{k, \text{specific}}$) of the designed catalyst can be calculated by dividing forward peak current of ethanol oxidation with Electrochemically active surface area (ECSA) of the catalyst.

$$\text{Specific Activity} = \text{Forward peak current} / \text{ECSA}$$

2.3.4 Methanol Oxidation Reaction (MOR)

The electrocatalytic activity of Pd/NrGO sheets, commercial 30% Pd/C, and commercial 40% Pt/C towards MOR was studied by Cyclic Voltammetry (CV) technique. The CV measurements

for MOR were obtained in N₂-saturated 1 M CH₃OH + 1 M KOH solution, and the potential was scanned from 0.3 to 1.5 V (vs RHE) at a scan rate of 50 mV s⁻¹. The scan was repeated several times to ensure that a stable CV was obtained. The stability of electrocatalyst was evaluated by chronoamperometry at a potential corresponding to the forward peak current for 3600 s in a freshly made electrolyte solution containing 1 M CH₃OH and saturated with N₂.

2.3.5 Oxygen Reduction Reaction (ORR)

The electrocatalytic activity of Pd/NrGO sheets, commercial 30% Pd/C towards ORR was studied by Linear Sweep Voltammetry (LSV) technique. The linear sweep voltammograms (LSV) were recorded in O₂ saturated 0.1 M KOH at room temperature at a scan rate of 10 mV s⁻¹ using a rotation rate of 1600 rpm. LSV plots were also recorded in N₂ saturated 0.1M KOH with same scan rate and used for elimination of the background current. For the calculation of Mass and specific activities, firstly, ORR LSVs were recorded at different rotation speed of 400,800,1600,2000,2400 rpm as shown in Figure. The kinetic current was estimated from this plot by using Koutecky-Levich (KL) equation as follows:^[60]

$$\boxed{1/I = 1/I_k + 1/I_d}$$

Where, I, I_k and I_d are experimentally measured current, kinetic current and diffusion limited current respectively. I_d can be obtained from the Levich equation:

$$\boxed{I_d = 0.62 nFA D^{2/3} \nu^{-1/6} \omega^{1/2} C_{O_2}}$$

where n = the number of electrons involved in the reaction,

F = Faraday's constant (96485 C/mol),

A = Area of the working electrode (which is 0.0707 cm² for 3mm GC-RDE)

D is the O₂ diffusion coefficient in the given electrolytic solution (for 0.1 M KOH solution it is 1.9 x 10⁻⁵ cm² s⁻¹,

ν is the kinematic viscosity of the given electrolyte (for KOH it is 1.01 x 10⁻² cm² s⁻¹),

ω is the angular frequency of rotation and is given by the formula, $\omega = 2 * \pi * f / 60$, where f is the rotation rate of RDE in rpm, and

C_{O₂} is the concentration of O₂ in 0.1 M KOH solution (1.21 x 10⁻⁶ molcm⁻³).

To determine the mass activity and specific activity of the designed electrocatalyst can be determined by using the slope and intercept of plot of $1/I$ vs. $\omega^{1/2}$

Using slope and intercept of KL-plot of $1/I$ vs. $\omega^{1/2}$ we can determine kinetic current (I_k) and number of electron transfer involved in the oxygen reduction reaction, respectively.

Mass activity ($I_{k, \text{mass}}$) can be calculated by dividing kinetic current with mass loading of noble metal (Pd or Pt) at 0.9 V vs. RHE.

Specific Activity ($I_{k, \text{specific}}$) was determined by normalising kinetic current with ECSA (Electrochemically Active surface area) at 0.9 V vs. RHE.

From the slopes of the KL- plot at the various applied potentials we can determine that ORR reaction follows the first order reaction kinetics. With the help of electron transfer number (n) one can confirm a complete reduction of O_2 to water on the catalyst surface.

Chapter 3

Results and discussions

This work is subdivided into three main parts. Our main aim is to synthesise noble metal-based nanocomposite and further explore their catalytic properties and stability for energy conversion and storage. Our main aim is to synthesize Noble Metal (Pd) based nanocomposite with NrGO (Nitrogen doped-reduced Graphene Oxide) and to further investigate their potential electrocatalytic applications as well as stability for various electrochemical reactions like Ethanol Oxidation Reaction (EOR), Methanol Oxidation Reaction (MOR), Oxygen Reduction Reaction (ORR) etc. The stability test of synthesised catalyst material was performed by using chronoamperometry measurements.

3.1 Synthesis of Palladium nanocomposite on Nitrogen-doped reduced Graphene oxide (NrGO) sheets

Several factors play a crucial role in regulating the size and distribution of nanoparticles on the support material. While one factor favours uniform particle distribution, another might lead to the aggregation of particles or cluster formation on the support material. All the parameters are optimized to achieve uniform distribution of noble metal nanoparticles on the support material.

3.1.1 Synthesis of Support Material (NrGO)

The present protocol for preparing NrGO involves three steps. At first, graphite oxide (GO) was prepared by a modified Hummer's method. In a typical synthesis, 133 ml of 9:1 mixture of conc. $\text{H}_2\text{SO}_4/\text{H}_3\text{PO}_4$ was slowly added to a beaker containing 1 g of graphite powder and 6 g of KMnO_4 placed on an ice bath to maintain the solution temperature below 10°C . Afterwards, the reaction mixture was heated at 55°C for 12 h with constant stirring. It was observed that after 12 hrs, the green colour solution was turned to dark brown. The reaction mixture was then cooled to room temperature, followed by the addition of 130 g of ice and 1 ml of H_2O_2 (30%), which immediately changed the colour of the solution to yellow, indicating the formation of

GO. The reaction mixture was then washed in succession with 200 ml water, 200 ml HCl (30%), 200 ml ethanol and 200 ml ether by repeated sonication and centrifugation. Finally, the product was precipitated in diethyl ether and dried in an oven at 60°C overnight. In the second step, to prepare nitrogen-doped graphene oxide from graphite oxide, 1.2 g of GO and 6 g of melamine ($C_3H_6N_6$) were dispersed in 100 ml and 400 ml of water, respectively, under sonication. Melamine suspension was then added to GO dispersion and kept under constant stirring for 12 hrs. Then the solution temperature was raised to 55 °C to evaporate the water. The dried sample was well grounded using a mortar pestle and pyrolyzed inside a tube furnace under an Ar atmosphere (with a heating rate of 5 °C min⁻¹) at 350 °C for 3 h and subsequently at 1000 °C for 30 min to get NrGO from NGO. Finally, the furnace was naturally cooled to room temperature, and NrGO samples were collected. Figure 11 and 12 illustrates the overall synthesis procedure of NrGO and the collected reaction product, respectively.

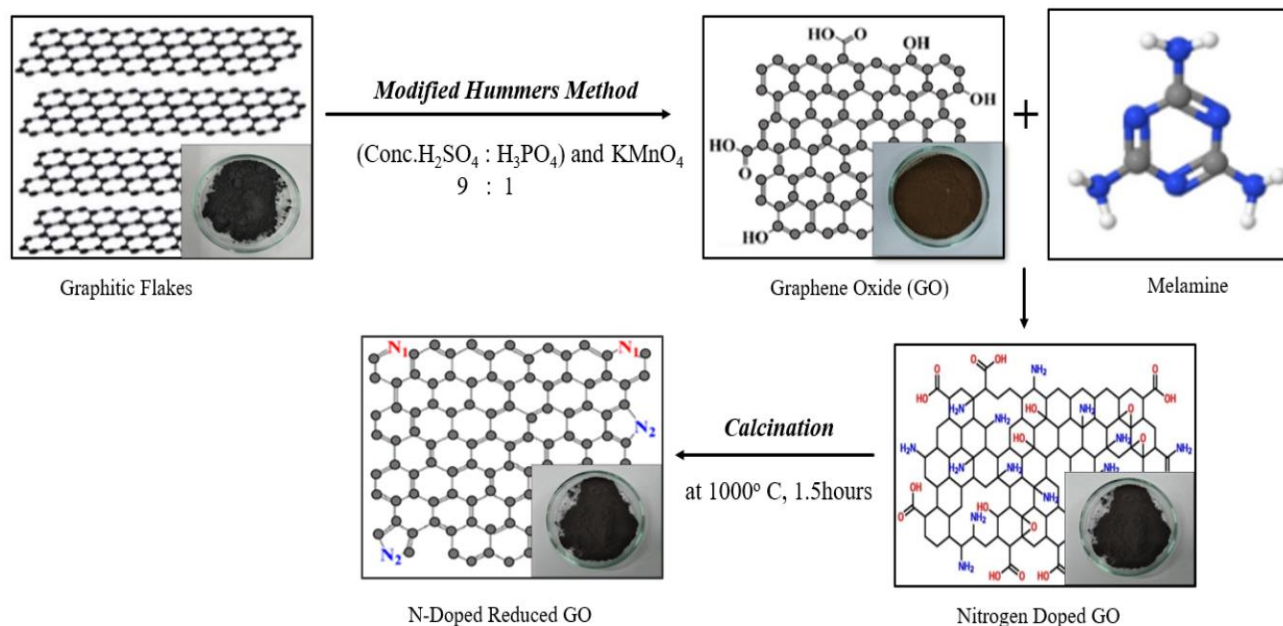


Figure 14. Schematic illustration for the synthesis of Nitrogen-doped reduced graphene oxide (NrGO)



Figure 15. Nitrogen-doped reduced graphene oxide (NrGO) in Alumina boat

3.1.2 Synthesis of Palladium nanocomposite supported on N-doped reduced graphene oxide sheets (Pd/NrGO)

The catalyst was synthesised by chemical reduction method and room temperature stirring method. The most frequently applied and reliable method of noble metal nanoparticles (NMNPs) synthesis is chemical reduction.^[61] The noble-metal nanoparticle composite was synthesised at room temperature using water as a solvent by simple chemical reduction method with NaBH₄ as a reducing agent. In the chemical reduction method, precursors dissolved in a solvent are reduced using reducing agents, and the resulting compound is stabilised, as shown in Figure.12. Borohydrides, amino boranes, hydrogen, acetylene, formaldehyde, hydrazine, hydroxylamine, polyols, citric and oxalic acids, sugars, hydrogen peroxide, carbon monoxide, and many more can all be utilised as reducing agents in the chemical reduction method. ^[62]

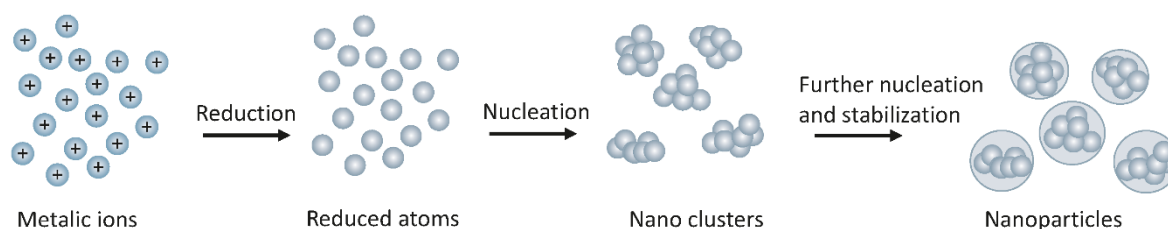
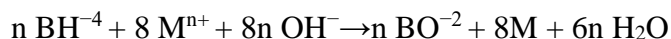


Figure 16. Schematic of reduction of metal ions in solution ^[63]

The choice of reductant is dictated by the conditions in which the reaction is carried out because the pH of the solution strongly conditions the activity of reducing agents. ^[64] One of the most potent inorganic reductants, sodium borohydride can be used to reduce the cations of noble metals like gold ^[65], silver ^{[66], [67]}, platinum ^[68], palladium ^[69], rhodium, ruthenium, osmium, and iridium to their nanosized elemental state, as shown in the equation below ^[64].



In the typical synthesis procedure, 15 mg of NrGO was first dispersed in 10 ml of water by stirring for 2 hrs. Then 5 ml, 0.15 mmol Metal precursor solution (K_2PdCl_4 for Pd) was prepared using water and 2M HCl. The metal precursor solution was added dropwise to the NrGO dispersion, and the resulting mixture was stirred for 2.5 hrs. at 1000 rpm. 4 ml, 0.5M NaBH_4 solution was then slowly added to the reaction mixture under ice-cold conditions. Finally, the reaction mixture was stirred at 1000 rpm for 12 hr overnight. The sample was collected by centrifugation and washed several times with water and ethanol, and dried in an oven at 60 °C.



Figure 17. Schematic representation of reaction setup for synthesis of metal nanoparticles composites on NrGO.

3.1.3 Role of Support Material

The support for electrocatalysts for DAFCs can significantly affect the utilization of noble metals and the catalytic activity of an electrocatalyst. An ideal electrocatalyst support should possess a high surface area and superior conductivity to promote the transport of electrons for better charge efficiency. The support materials typically comprise carbonaceous materials, for

example, activated carbon, graphene, carbon nanotubes, and non-carbonaceous materials, such as mesoporous silica and metal-oxides. Overall, the critical properties of support materials for practical applications are listed below:^[70]

- 1) It should have good electrical conductivity.
- 2) There should be some strong interaction/link between the support and the catalyst.
- 3) It should possess a high surface area to enhance the catalytic activity of an electrocatalyst.
- 4) It must have acceptable resistivity towards corrosion.

Recently, nitrogen-doped carbon materials have gained the attraction of researchers to use as support material because of the ability of the nitrogen doping on the carbon support to promote the stability and electrocatalytic activities of Pt and Pd-based catalysts.^[71]

In this work, nitrogen-doped reduced graphene oxide (NrGO) has been utilized as a support material because :

1. N-doped graphene oxide is proper to use as a supporting material because it has a high surface area than pristine graphite due to the exfoliation of graphitic layers.
2. The N-doped graphene sheets had a more disordered structure than rGO due to nitrogen doping. The graphite structure contains a stack of carbon with sp^2 hybridization and one delocalized π electron. In NrGO while, the stacks of carbon were extended, and free π electrons can easily delocalize across the layer which helps in charge transfer and plays a role in increasing the catalytic activity
3. Three standard bonding configurations of N atoms in graphene are demonstrated for N-doped graphene, including pyrrolic, pyridinic, and graphitic (or quaternary) N. By depositing the Pd atom on the surface of NrGO, we can create a strong between the Pd atom and the pyrrolic nitrogen moiety of NrGO. The Pd-N bond gets strengthened in the presence of oxygen-containing functional groups accompanied by a charge transfer from the 3d orbitals of Pd to the 2p orbitals C ,N and O. This charge transfer helps in lowering the binding energy of Pd, which in turn helps in enhancing its electrocatalytic activity.
4. Nitrogen doping increases the basicity of the attached graphitic carbon due to the lone pair of electrons of pyridinic-N species, stabilising the carbon against oxidation and facilitating oxygen reduction by delocalising on the conjugated system of sp^2 -hybridised carbon frameworks.

5. Their d-band vacancy can be increased after alloying and deposition of catalyst material on the support which in turn leads to the strong metal-O₂ interaction. Therefore, the ORR mechanism of alloy formation can break the oxygen bond leading to a completed 4-electron reduction.^[72]

3.1.4 Optimization of temperature of NaBH₄ addition

To see the effect of temperature on the nanoparticles distribution on the support material, a similar synthesis procedure was carried out but with the addition of a reducing agent at room temperature. For that, 15 mg of NrGO was first dispersed in 10 ml of water by stirring for 2 hrs. Then 5 ml, 0.15 mmol Metal precursor solution (K₂PdCl₄ for Pd) was prepared using water and 2M HCl. The metal precursor solution was then added dropwise to the NrGO dispersion. The resulting mixture was stirred for 2.5 hrs. at 1000 rpm. 4 ml, 0.5M NaBH₄ solution was slowly added to the reaction mixture at room temperature. Finally, the reaction mixture was stirred at 1000 rpm for 12 hr overnight. The prepared sample was collected by centrifugation, washed several times with water and ethanol, dried in an oven at 60 °C and subjected to further characterization.

3.1.5 Overview on optimum conditions for obtaining uniform distribution of nanoparticles on support material

In order to get the uniform particle distribution over the surface of Nitrogen-doped reduced graphene oxide, it was observed that the temperature at which a reducing agent like NaBH₄ was added to the reaction mixture plays a vital role in the distribution of the particles over the support material. It was experimentally found that if a reducing agent like NaBH₄ was added to the reaction mixture under ice-cold conditions at 0 C, then only we would get a homogeneous and uniform distribution of particles over the surface of the support material. This effect of temperature at which NaBH₄ addition was confirmed by carrying out a similar reaction but with NaBH₄ addition at room temperature and formation of small clusters, particle agglomerates, and inhomogeneity in particle distribution confirms that for the better activity of the catalyst, NaBH₄ should be added under ice-cold conditions during the synthesis.

3.2 Characterization of designed electrocatalyst (Pd loaded on NrGO)

3.2.1 Transmission Electron Microscopy-image Analysis

Electron microscopic analysis of the N-doped reduced graphene oxide (NrGO), obtained by thermal treatment of graphene oxide (GO) shows the formation of flake-like thin transparent sheets depicting a greater extent of exfoliation (Figure 18). The high-resolution TEM images (HR-TEM) displayed an inter-planar spacing of 0.35 nm corresponding to the (002) planes of NrGO.

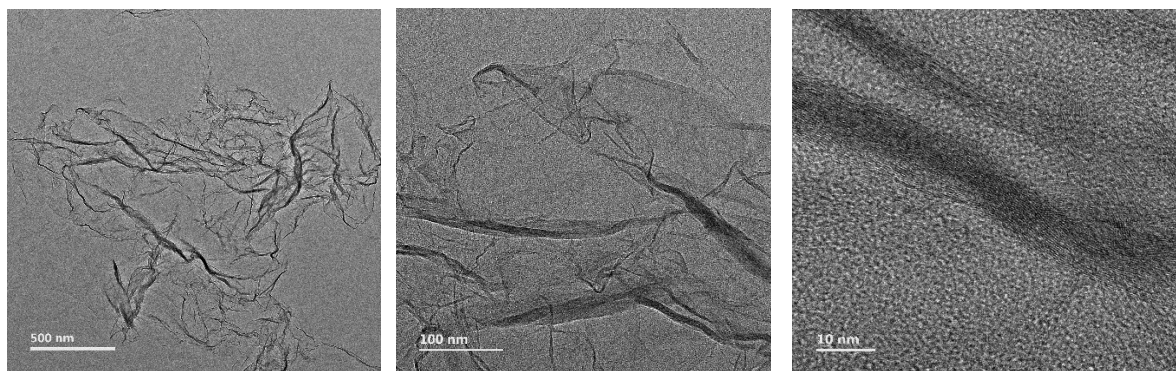


Figure 18. Microscopic characterization of NrGO : (a,b) TEM image at low resolution (c) high-resolution TEM image depicting (002) planes.

We synthesised Pd/NrGO using chemical reduction method by just simply mixing metal precursors with support solution by using some reducing agent like NaBH_4 . A typical High-resolution TEM images (HR-TEM) of Pd particles on NrGO shows the lattice fringes with an inter-planar spacing of 0.22 nm corresponding to the (111) planes of FCC Pd crystal. Nearly spherical 3.5 nm Pd nanoparticles were deposited on the NrGO support by chemical reduction method using NaBH_4 as reducing agent. The corresponding particle-size distribution is given in figure 19 below. Careful observation of TEM images confirmed that the particles are uniformly distributed over the NrGO sheets without forming clusters.

The diffraction rings in the SAED pattern also shows the presence of FCC phase of Pd particles.

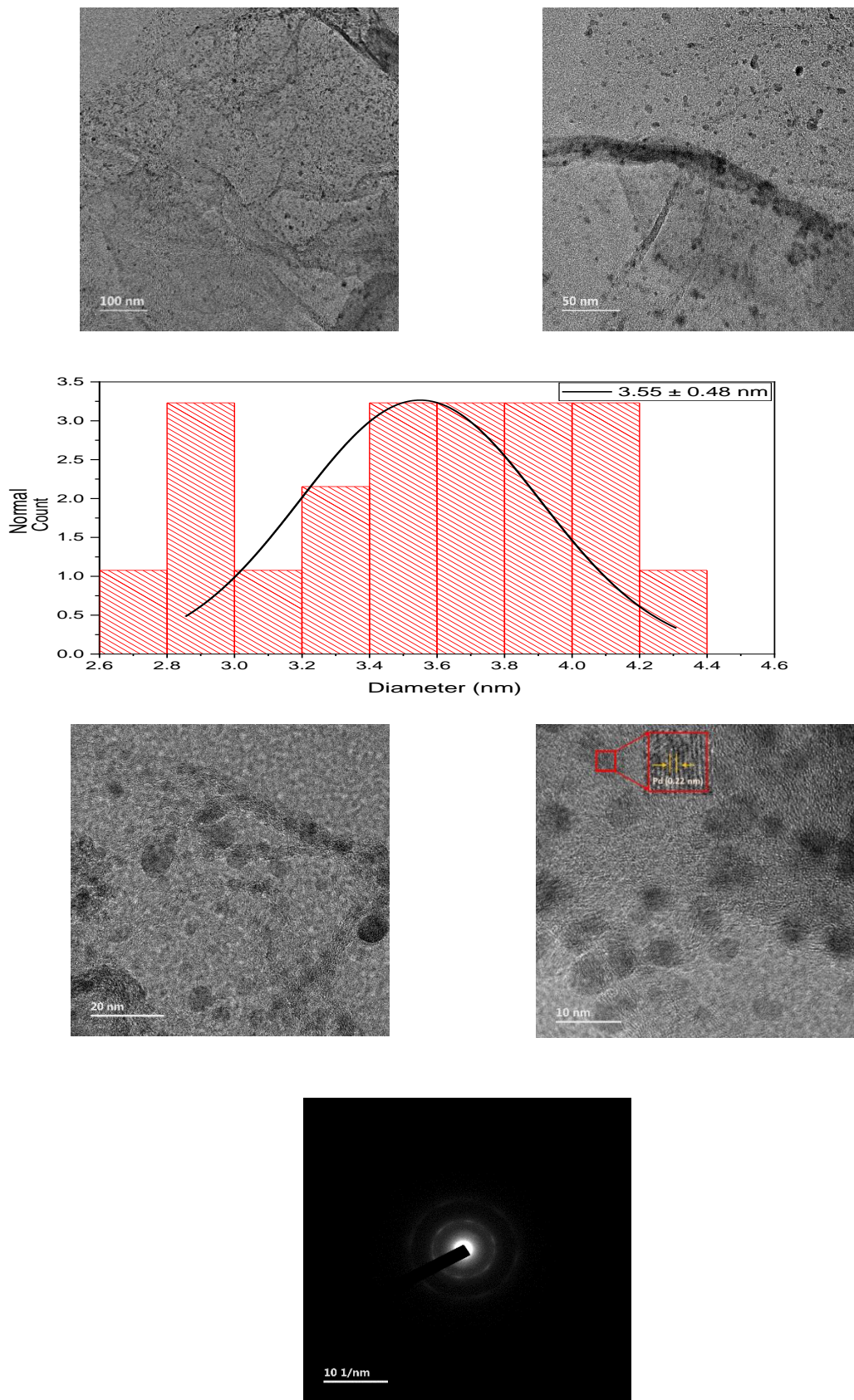


Figure 19. Microscopic characterization of Pd/NrGO (30% loading) : (a,b) TEM image at low resolution (c) the particle size distribution, (d) high-resolution TEM image, (e) corresponding SAED Pattern.

In order to understand the effect of reducing agent addition on size distribution of Pd nanoparticles on an NrGO surface, we performed a same synthesis but with NaBH₄ addition at room temperature. It was observed that due to NaBH₄ addition at room temperature the particle distribution was not that uniform over the NrGO surface as it was in earlier case when NaBH₄ was added under ice cold conditions. From careful TEM image analysis, it was confirmed that the particles were not much uniformly distributed over the NrGO sheets and form some agglomerates and small clusters.

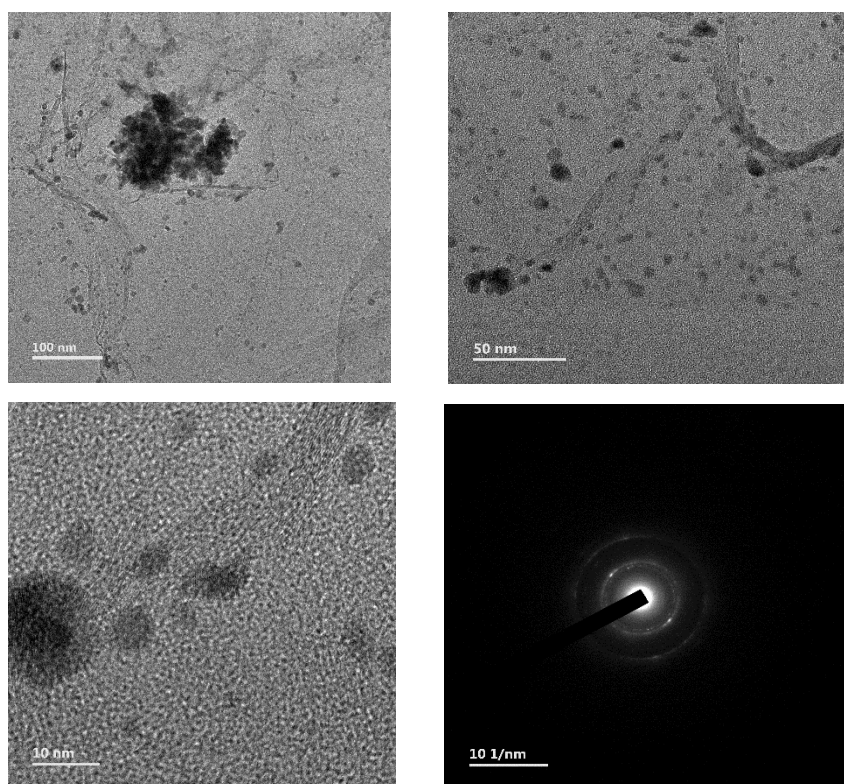


Figure 20. Microscopic characterization of Pd/NrGO (30% loading) with NaBH₄ addition at room temperature: (a,b) TEM image at low resolution (c) high-resolution TEM image, (d) corresponding SAED Pattern

3.2.2 Energy Dispersive Spectroscopy

We have also performed EDS elemental mapping analysis on the same region to confirm a consistent distribution of Pd, C and N in the Pd/NrGO framework. The presence of Pd metal on NrGO can also be determined using EDS-analysis.

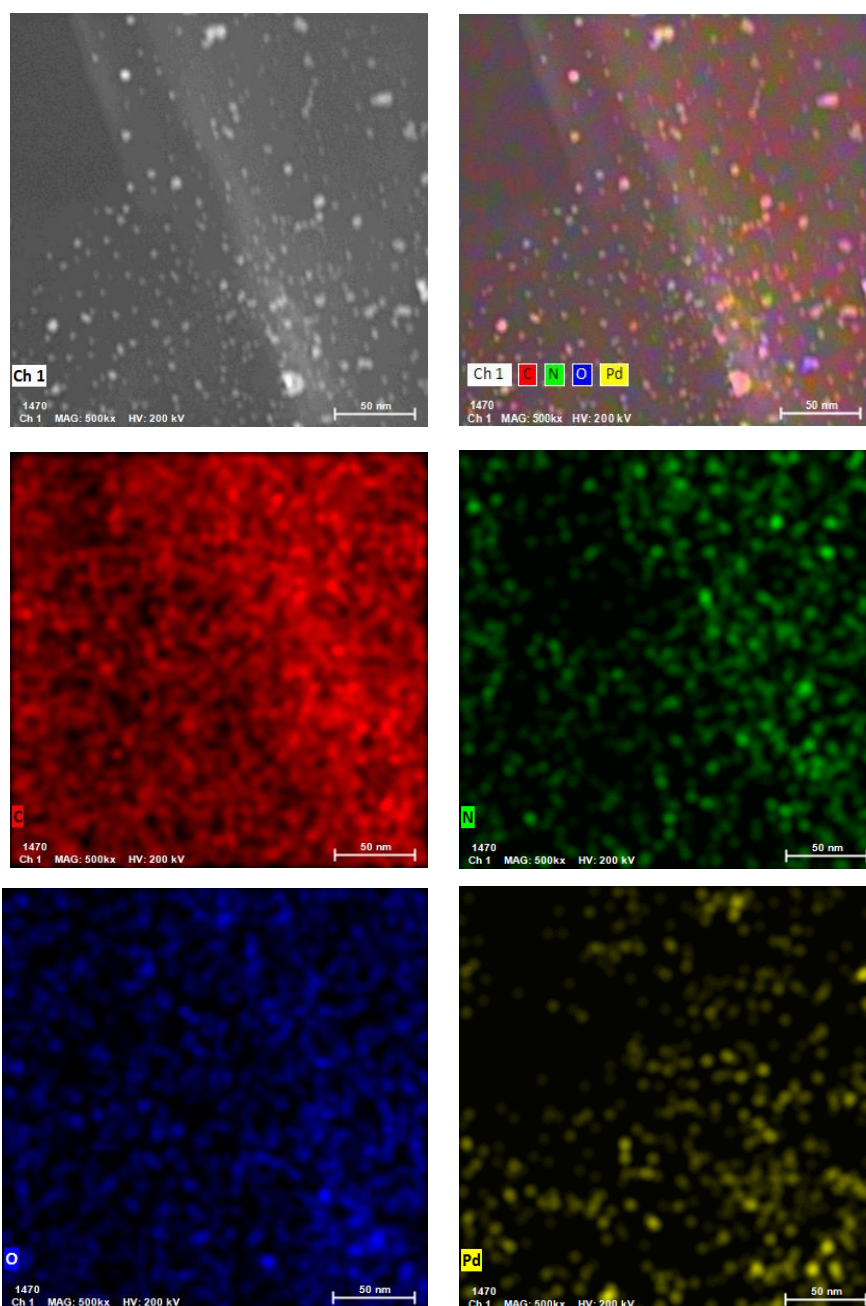


Figure 21. Pd/NrGO corresponding energy dispersive X-ray spectroscopic elemental mapping images.

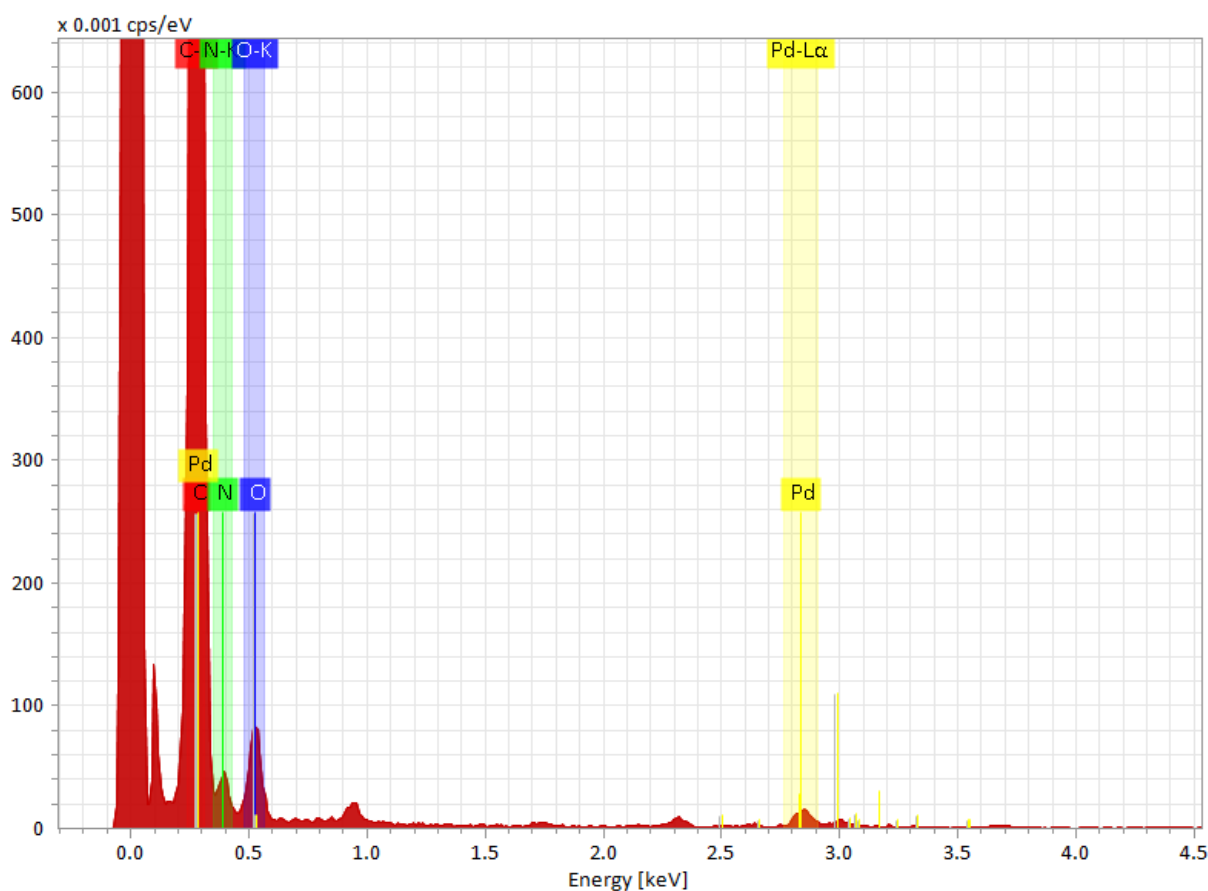


Figure 22. Corresponding energy dispersive X-ray spectra for Pd/NrGO.

3.2.3 Powder X-ray diffraction (P-XRD) Analysis

Powder X-ray diffraction patterns were recorded for all the samples in order to confirm the phase purity of metal nanoparticles (Figure 23). A diffraction peak at 9.3° for graphene oxide (GO) was observed for the (001) basal plane with a larger spacing of 0.86 nm vs. graphite due to the presence of oxygen functionalities.^[73] The peak in NrGO shifted to 26.4° compared to GO due to reduction of the functional groups during the synthesis process. In Pd/NrGO the peaks at 26.4° is assigned to (002) basal plane of NrGO and peaks corresponding to 40° , 46.2° and 67.5° were assigned to (111), (200) and (220) crystal planes of palladium with FCC crystalline structure as shown in Figure. 23 below.

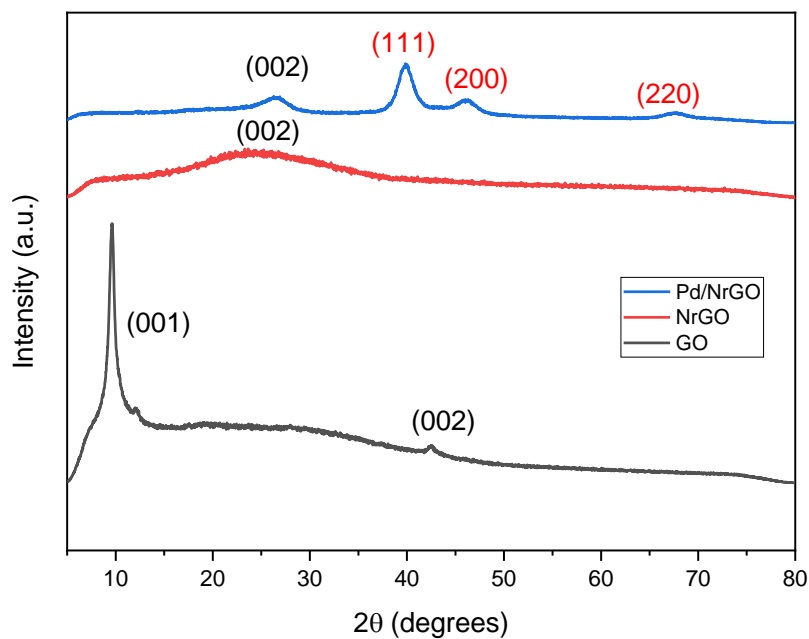


Figure 23. PXRD patterns of graphene oxide (GO), Nitrogen-doped reduced graphene oxide (NrGO) and Pd/NrGO (30% metal loading)

The peaks corresponding to Pd in Pd/NrGO suggests d-spacing value of Pd/NrGO was in good agreement with HR-TEM observation.

3.3 Ethanol Oxidation Reaction (EOR)

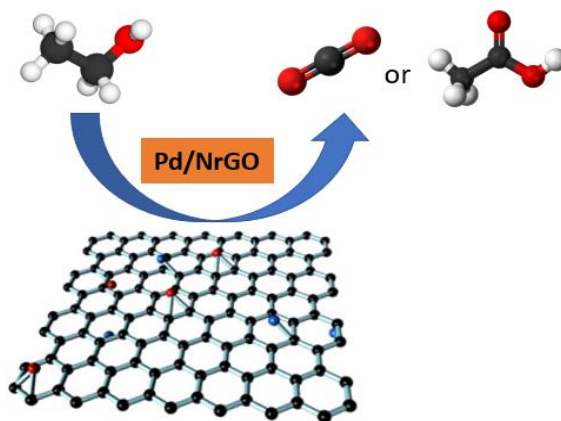


Figure 24. Schematic of Ethanol electrooxidation on Pd/NrGO surface

3.3.1 Electrocatalytic EOR Performance

The efficiency of the Pd/NrGO metal nanocomposite was employed as an anodic ethanol oxidation reaction (EOR) and compared with commercial catalyst 30% Pd/C. EOR was evaluated in Ar saturated 1M KOH solution containing 1M EtOH in the potential window of 0.3 to 1.5 V (vs RHE) with a scan rate of 50 mV/s at the room temperature. Figure below shows typical EOR-CV plots obtained for Pd/NrGO nanocomposite and Pd/C during ethanol oxidation.

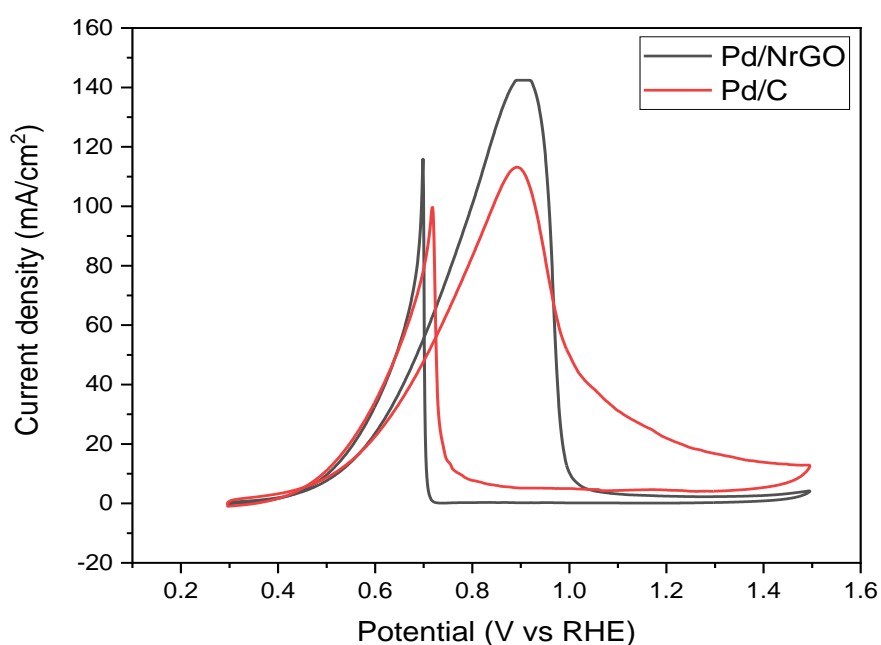


Figure 25. Cyclic Voltammograms for electro-oxidation of ethanol using Pd/NrGO and Pd/C

Among them, Pd/NrGO exhibits much higher anodic peak current of 10.06 mA which is higher than Pd/C (8 mA). It can be observed that the, Pd/NrGO demonstrates the highest mass activity of 0.711 mA/ug which is 1.25 times higher than that of Pd/C (0.565 mA/ug). At the same time, the specific activity of Pd/NrGO was estimated to be 15.71 mA/m² which is 2.11 times higher than Pd/C (7.43 mA/m²). The plots for mass activity and specific activity are shown below in figure. 26 and 27.

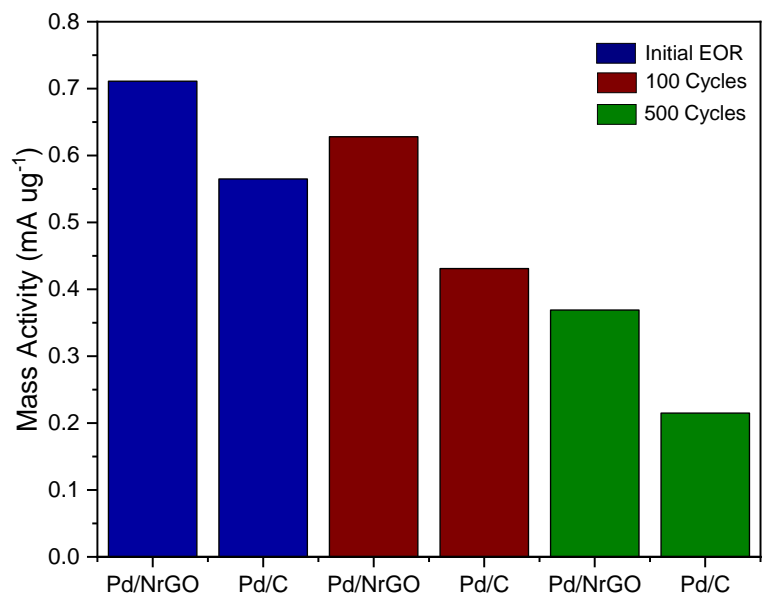


Figure 26. Histograms showing mass activity for electro-oxidation of ethanol using Pd/NrGO and Pd/C.

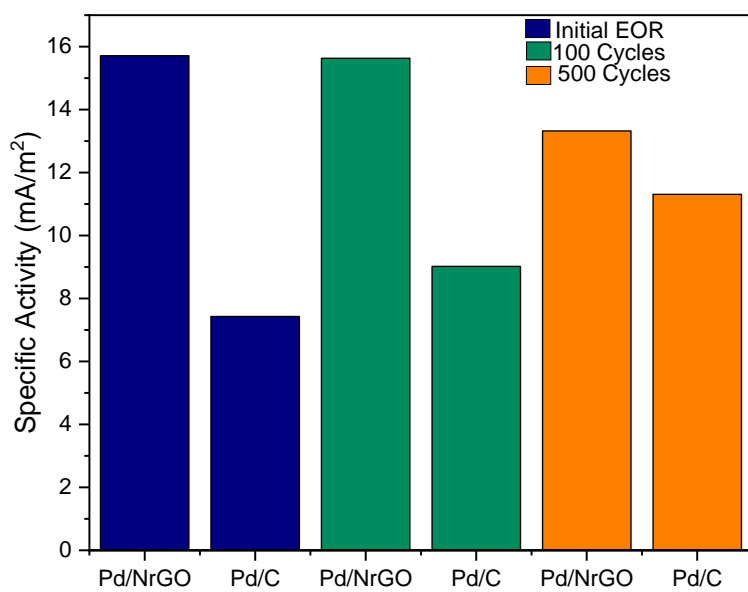


Figure 27. Histograms showing specific activity for electro-oxidation of ethanol using Pd/NrGO and Pd/C.

3.3.2 Stability of the Catalyst Material

We have further investigated the stability of Pd/NrGO for EOR by performing CV cycling in the potential range 0.5 V to 1.2 V vs. RHE with a scan rate of 100 mV/s as shown in the Figure 34 below. It could retain 51.37 % of its initial mass activity even after 500 potential cycles which is much better stability possessed by many other states of the art catalyst developed in the recent past (Stability comparison table 1.1) .This suggest that Pd/NrGO exhibits excellent durability along with enhanced activity.

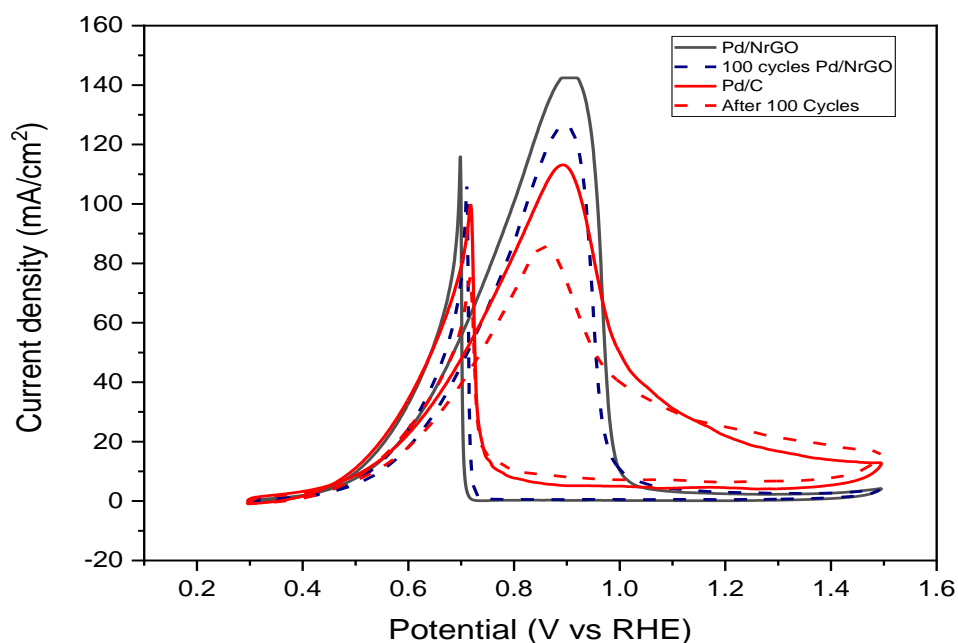


Figure 28. Pd/NrGO and Pd/C MOR stability up to 100 cycles with a scan rate of 100 mV/s

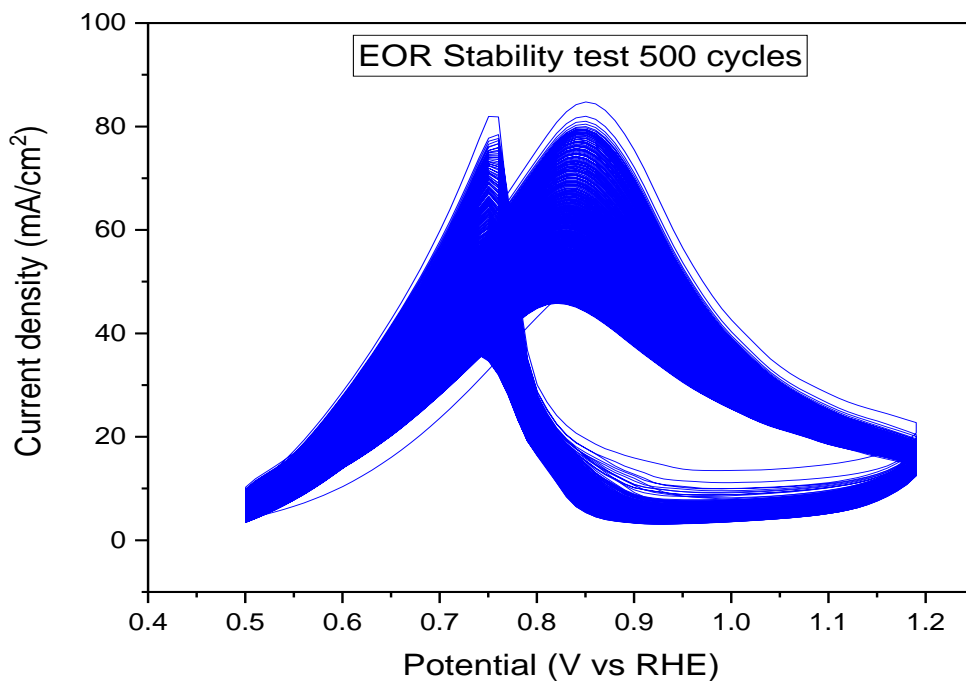


Figure 29. Pd/C EOR stability test for 500 cycles with a scan rate of 100 mV/s

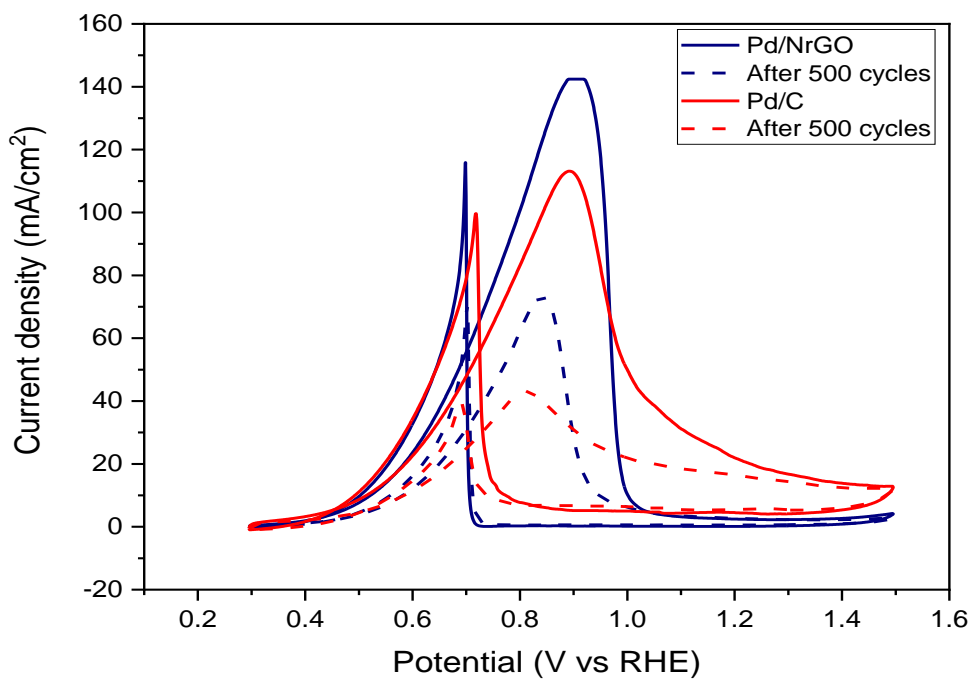


Figure 30. Pd/NrGO and Pd/C MOR stability up to 500 cycles with a scan rate of 100 mV/s

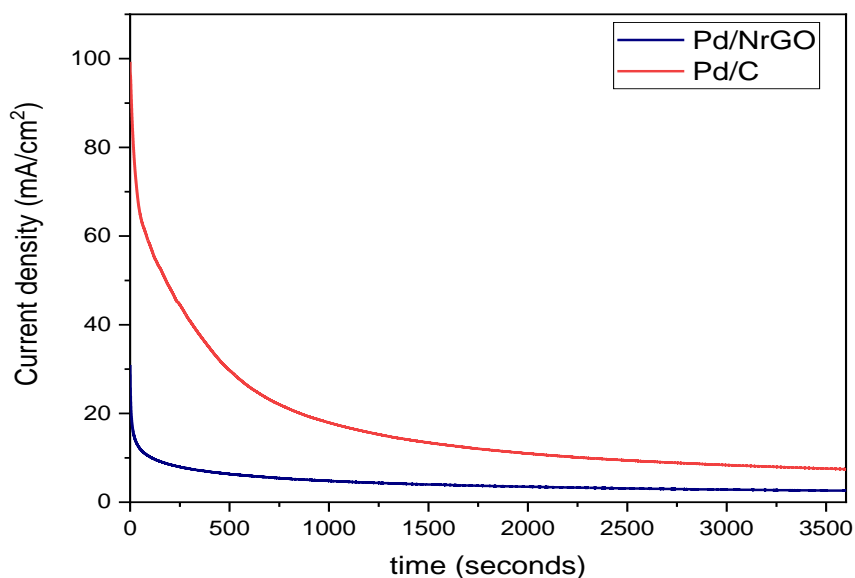


Figure 31. The chronoamperometry curves for Pd/NrGO and Pd/C up to 3600 sec during ethanol oxidation reaction.

3.3.3 Comparison of EOR performance with literature Work

A comparison of these activity parameters with the other recently developed state-of-the-art catalysts shows that EOR activity of Pd/NrGO is high in Alkaline medium. (Table 1).

EOR Electrocatalyst	Electrolyte	Forward peak current density (mA/cm²)	Stability	References
Pd/NrGO	1M KOH + 1 M EtOH, RD-GCE	142.37	500 cycles	This work
Pd (20 wt%) /Ni-NSC	1M KOH + 1 M EtOH, GCE	110	1600 s	[74]
FePd-Fe ₃ C/MWCNTs	1M KOH + 1 M EtOH, GCE	84.8	1000 s	[75]
Pd-	1M KOH + 1 M EtOH,	30.5	2000 s, 350	[76]

W@Fullerene-C60	GCE		cycles	
Pd/Cu/Graphene	1M KOH + 1 M EtOH, GCE	26.6	3500 s	[77]
Pd _{1.6} Ni _{0.4} Ge	1M KOH + 1 M EtOH, GCE	13	350 cycles	[78]
Pd-S-HCNFs	1M KOH + 0.5M EtOH, GCE	9	6000 s	[79]
Pd ₂ Ge-36 NPS	1M KOH + 0.5M EtOH, GCE	4.1	1000 s,250 cycles	[80]
Pd Ag-NS	1M KOH + 1 M EtOH, GCE	2.4	1000 s	[81]
Pd-Ru/CNFs	1M KOH + 1 M EtOH, GCE	0.02	2000 s	[82]

Table 1. Comparison of EOR performance of Pd-based nanostructures developed in this thesis with recently reported literature data.

3.4 Methanol Oxidation Reaction (MOR)

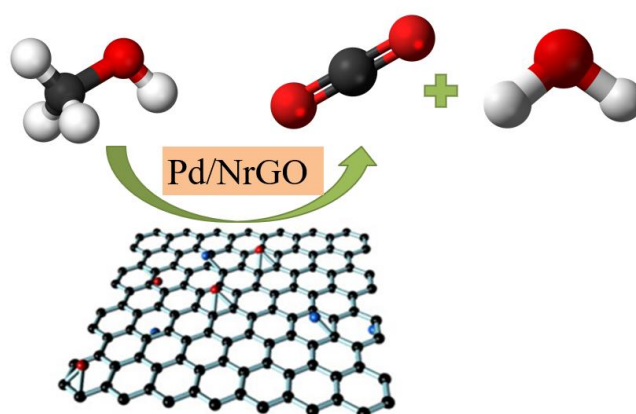


Figure 32. Schematic of Methanol electrooxidation on Pd/NrGO surface

3.4.1 Electrocatalytic MOR performance

The efficiency of the Pd/NrGO nanocomposite was also employed as an electrocatalyst for anodic methanol oxidation reactions (MOR) and compared with Pd/C. MOR was evaluated in Ar saturated 1M KOH solution containing 1M MeOH in the potential window of 0.3 V to 1.5 V (vs. RHE) with a scan rate of 50 mV/s at the room temperature. Figure 39 below shows MOR-CV plots obtained for Pd/NrGO and Pd/C during methanol oxidation.

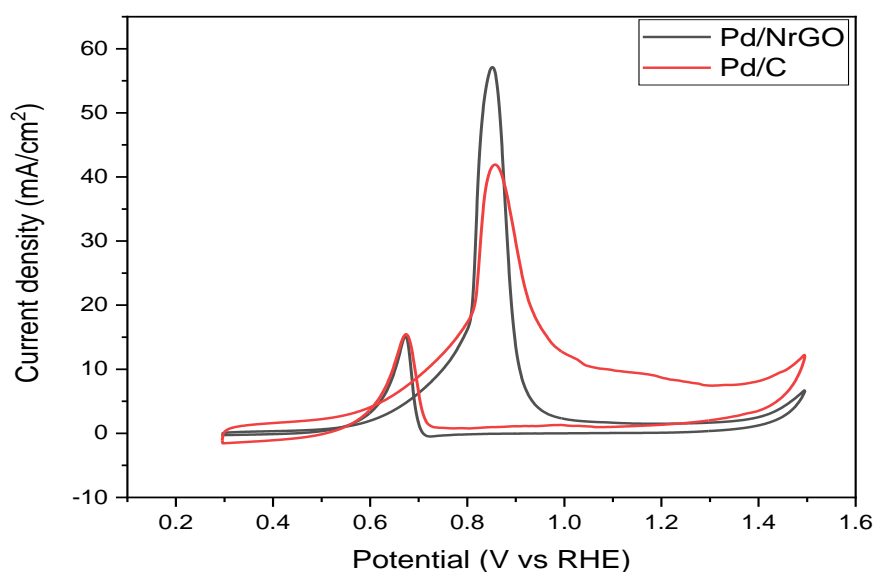


Figure 33. Cyclic Voltammograms for electro-oxidation of methanol using Pd/NrGO and Pd/C.

Among them, Pd/NrGO exhibits much higher anodic peak current as compared to Pd/C. It can be observed that the, Pd/NrGO demonstrates the highest mass activity of 0.286 mA/ug which is 1.36 times higher than Pd/C. At the same time, the specific activity of Pd/NrGO was estimated to be 6.948 mA/m² which is 2.73 times higher than Pd/C as shown in the Figure 35 below.

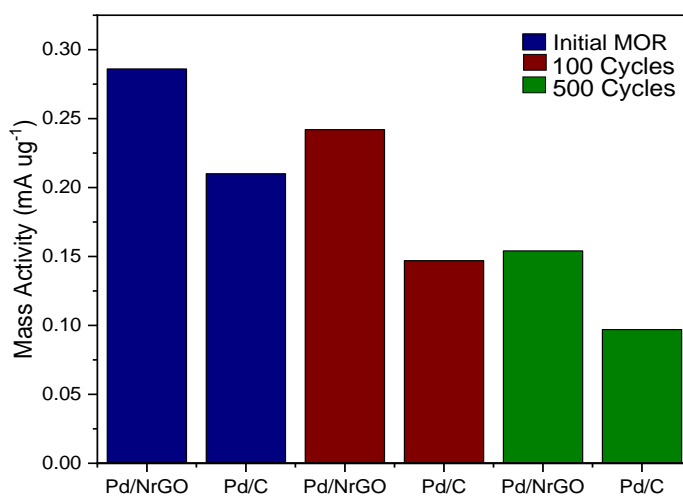


Figure 34. Histograms showing mass activities for methanol oxidation by Pd/NrGO and Pd/C.

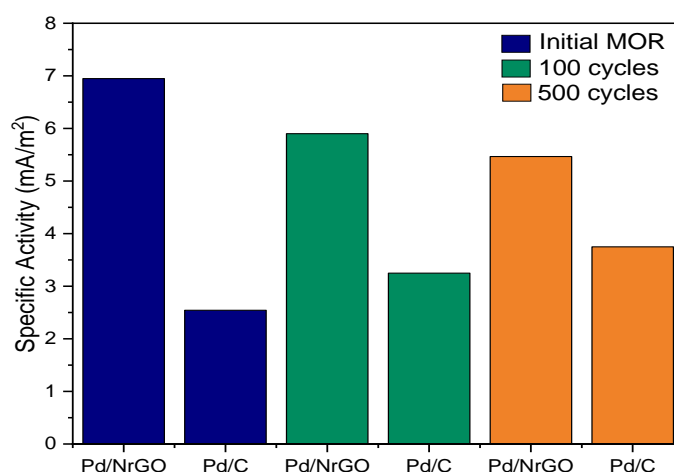


Figure 35. Histograms showing specific activities for methanol oxidation by Pd/NrGO and Pd/C.

The ratio of the forward to backward peak current (I_f / I_b) provides the estimation of poisoning tolerance factor of the electrocatalyst to the carbonaceous intermediates adsorbed on the catalyst surface formed during the partial methanol oxidation. Higher is the I_f / I_b ratio, better is the tolerance of the catalyst towards adsorbed carbonaceous intermediates. The I_f / I_b ratio of

Pd/NrGO is 3.73 , which is 1.37 times higher than that of Pd/C. This means that designed electrocatalyst shows a better tolerance towards carbonaceous intermediates.

All these results indicates that the MOR performance of Pd/NrGO nanocomposite is much superior to the commercial Pd/C.A comparison of these activity parameters with the other recently developed state-of-the-art catalysts shows that MOR activity of Pd/NrGO is high in Alkaline medium (Table 2).

3.4.2 Stability of the Catalyst Material

To check the stability of the Pd/NrGO nanocomposite for MOR we performed CV in the potential range of 0.5V to 1.2V vs. RHE with a scan rate of 100 mV/s as shown in Figure below. It could retain 53.33 % of its initial mass activity even after 500 potential cycle which is much better stability possessed by many other states of the art catalyst developed in the recent past (Table 1.2).This suggests that Pd/NrGO exhibits excellent durability along with the enhanced activity.

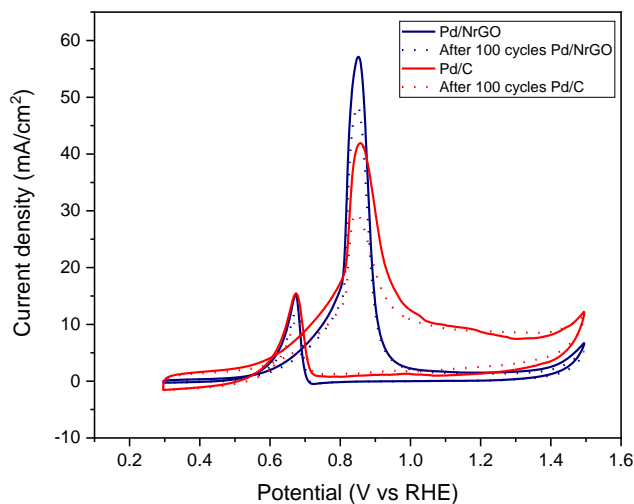


Figure 36. Pd/NrGO and Pd/C MOR stability up to 100 cycles with a scan rate of 100 mV/S

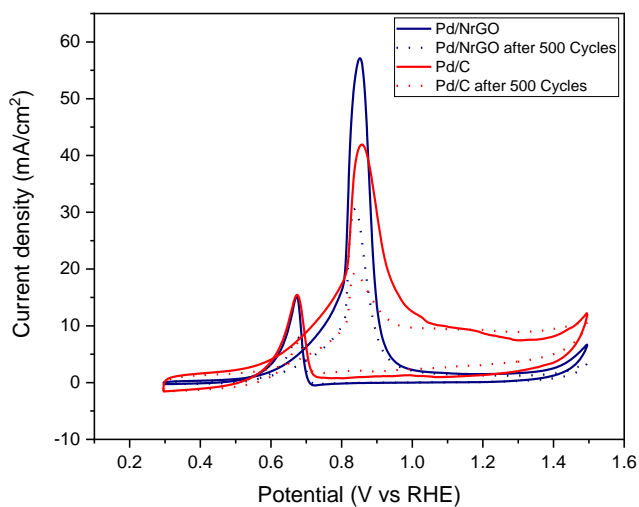


Figure 37. Pd/NrGO and Pd/C MOR stability up to 500 cycles with a scan rate of 100 mV/sec.

We finally examined the stability of catalyst for methanol oxidation by chronoamperometric measurement at the peak potential. From figure it can be observed that the stability of Pd/C is better as compared to Pd/NrGO even after 3600 s.

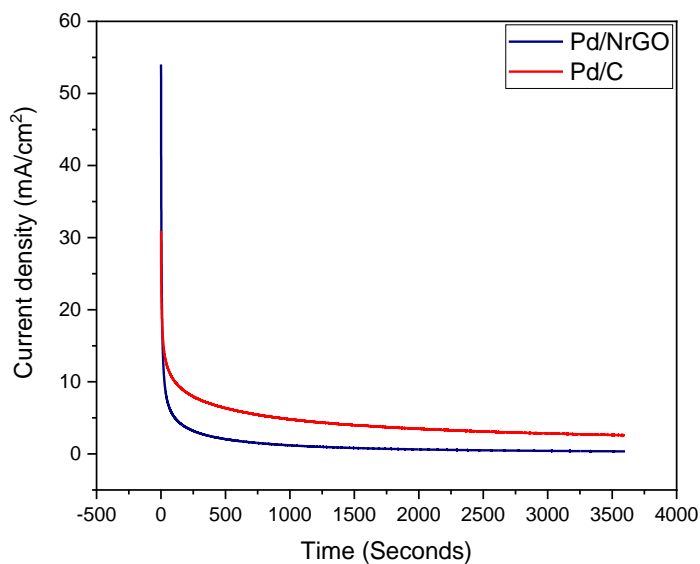


Figure 38. The chronoamperometry curves for Pd/NrGO and Pd/C up to 3600 sec during methanol oxidation

3.4.3 Comparison of MOR performance with literature Work

A comparison of these activity parameters with the other recently developed state-of-the-art catalysts shows that MOR activity of Pd/NrGO is high in Alkaline medium (Table 2).

MOR Electrocatalyst	Electrolyte	Forward peak current density (mA/cm ²)	Stability	References
Pd/NrGO	1.0 M KOH + 1 M CH₃OH, RD-GCE	57.27	500 cycles	This work
Pd-Cu Alloy	1.0 M NaOH + 0.5 M CH ₃ OH, GCE	46.5	600 sec	[83]
Pd/Cu ₃ P/rGO	1.0 M KOH + 1 M CH ₃ OH, GCE	33.9	3600 sec	[84]
Pd-4-Ni	1.0 M NaOH + 1 M CH ₃ OH, GCE	12.7	5000 sec	[85]
AuPd@Pd NCs/N-RGOH	0.5 M KOH + 1 M CH ₃ OH, GCE	11.5	-	[86]
Pd/TiO ₂ /Ti	1M KOH + 0.5 M CH ₃ OH, GCE	9.6	500 sec	[87]
PdNPs/3DNPG	1.0 M NaOH + 0.5 M CH ₃ OH, GCE	4.86	-	[88]
Pd-PtANFs/rGO	1.0 M NaOH + 0.5 M CH ₃ OH, GCE	2.16	-	[89]
Pd nanoparticles/GN	0.5 M NaOH + 0.5 M CH ₃ OH, GCE	1.858	-	[90]

G-Pd	1M NaOH + 1M MeOH, GCE	0.8	100 cycles	[91]
------	------------------------	-----	------------	------

Table 2. Comparison of MOR performance of Pd-based nanostructures developed in this thesis with recently reported literature data.

3.5 Oxygen Reduction Reaction (ORR)

3.5.1 Electrocatalytic ORR performance

The electrocatalytic ORR activity of Pd/NrGO was examined under alkaline conditions using Linear Sweep Voltammetry (LSV) and rotating disk electrode techniques. Commercial Pd/C was also used for both qualitative and quantitative comparison purpose. The ORR performance was evaluated by recording the LSV polarization curves in O₂ saturated 0.1M KOH at a scan rate of 10 mV/s at different rotation rates of 400, 800, 1200, 1600, 2000 and 2400 rpm using a GC-RDE.

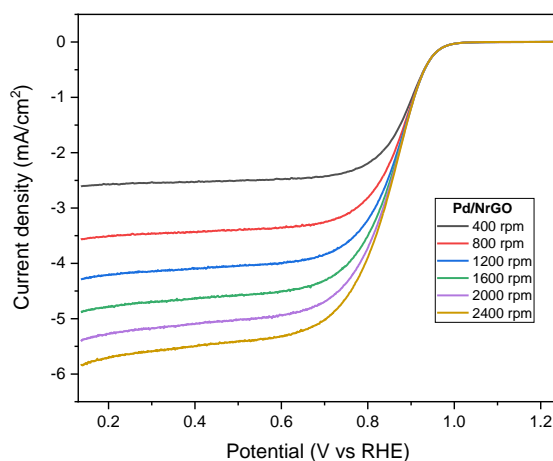


Figure 39. The ORR Polarization curves for Pd/NrGO (30% metal loading) in O₂ saturated 0.1 M KOH at different rotation rates of 400, 800, 1200, 1600, 2000 and 2400 rpm

As shown in Figure 40 the Pd/NrGO exhibited comparable ORR activity with a favourable onset potential of 1.02 V vs. RHE and a half-wave potential ($E_{1/2}$) of 0.91 V vs. RHE which is

comparable with half-wave potential of commercial Pd/C which is 0.92 V.

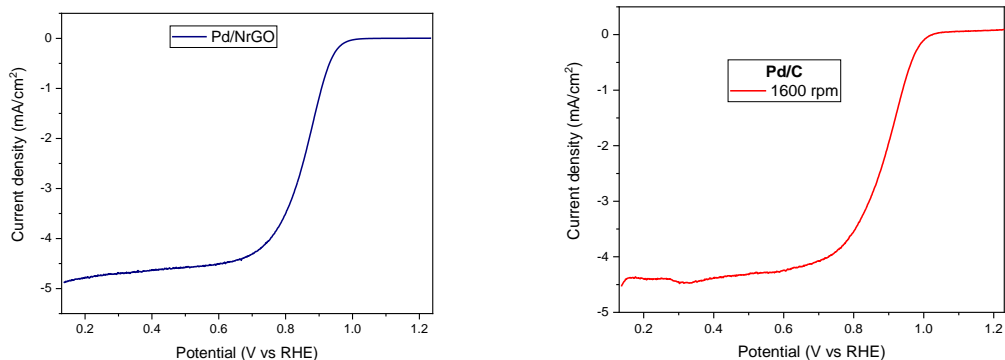


Figure 40. The ORR Polarization curves for Pd/NrGO (30% metal loading) and Pd/C in O₂ saturated 0.1 M KOH at the rotation rate of 1600 rpm.

The electrochemically active surface area (ECSA) that provides an estimate for the active sites present in the catalysts were calculated from the CV curves by quantifying the charge required during the Pd(OH)₂ reduction present on the surface of the catalyst. Herein, the ECSA for Pd/NrGO and Pd/C was estimated to be 5.75 m²/g and 12.11 m²/g respectively.

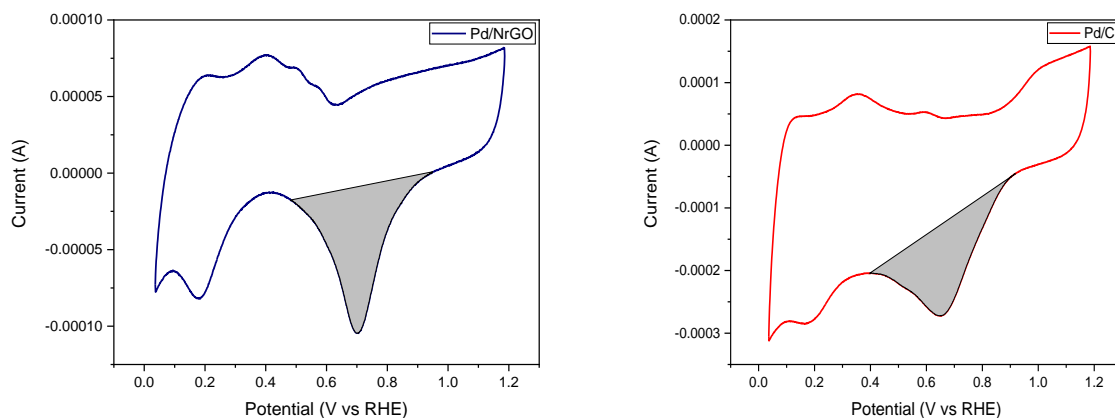


Figure 41. The recorded cyclic voltammograms for ECSA determination of Pd/NrGO and Pd/C respectively.

Furthermore, the ORR kinetic currents at 0.8 V vs. RHE of these samples were calculated using Koutecky - Levich (K-L) equation and the corresponding mass activities (I_k mass) and specific activities (I_k specific) were obtained by normalizing the kinetic current with noble metal loading on the electrode surface and the ECSA respectively.

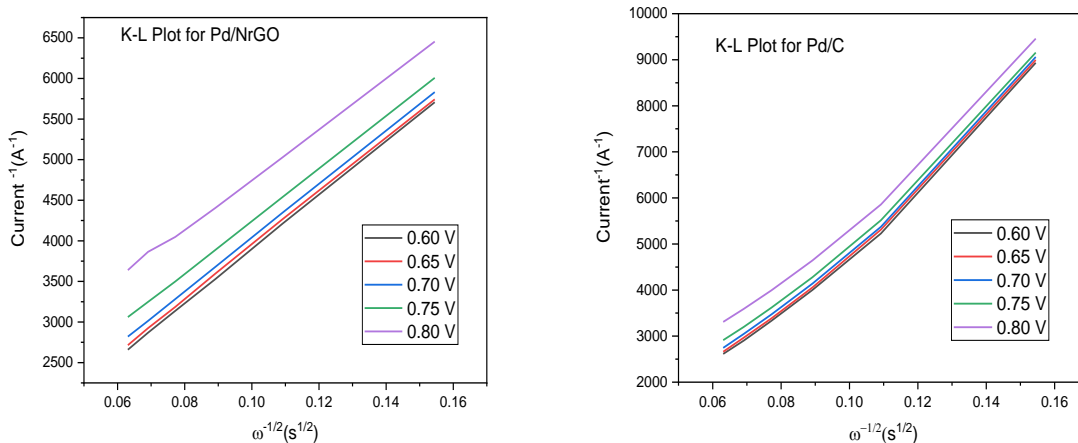


Figure 42. Koutecky - Levich (K-L) plot for Pd/NrGO and Pd/C, respectively.

It can be observed that the, Pd/NrGO nanocomposite demonstrates the highest specific activity of 7.219 mA/m^2 which is 1.45 times higher than Pd/C (4.975 mA/m^2). But, at the same time mass activity of Pd/C was estimated to be 0.602 A/mg which is 1.45 times higher than that of Pd/NrGO (0.415 A/mg).The plot for specific activity and mass activity for both the catalysts were shown in Figure 43.

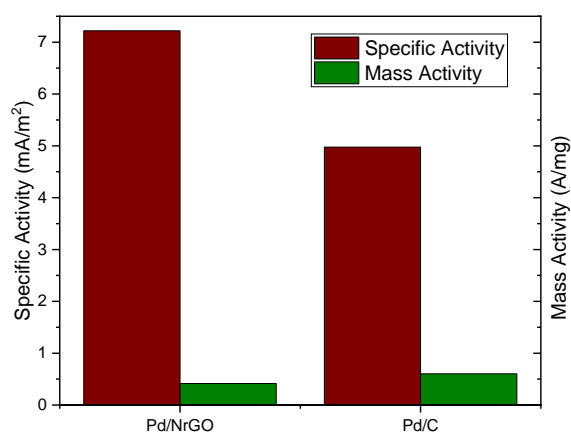


Figure 43. Histogram showing mass and specific activities for oxygen reduction reaction (ORR) by Pd/NrGO and Pd/C.

Chapter 4

Conclusions

Developing economically affordable, efficient, and robust fuel cell materials is vital for commercialization. Due to their heterogeneous nature, Pd nanostructures are imperative catalysts for various electrochemical processes. Pd-based nanostructure's catalytic activity can be related to their size, morphology and composition.

We demonstrated a protocol for developing a promising electrocatalyst Pd/NrGO. This electrocatalyst consists of NrGO nanosheets decorated with Pd nanoparticles (approx. 3.5 nm size). A simple chemical reduction method has been used to synthesize the electrocatalyst in which NaBH_4 was used as a reducing agent. The in-situ deposition of carbon-based support is better than ex-situ deposition or deposition of pre-formed nanocrystals because of the minimal effect of the shear forces acting during deposition.

The catalyst Pd/NrGO exhibits excellent electrocatalytic activity and stability towards alcohol oxidation reaction (like EOR and MOR) and a comparable ORR activity in comparison with commercial catalyst Pd/C. It was found that Nitrogen doping creates large quantities of pyrrolic-N in graphene, and the bonding of pyrrolic nitrogen with metal helps in generating many active and stable electrocatalysts.

Thus, we designed a cost-effective bifunctional electrocatalyst for Direct Alcohol fuel Cells (DAFCs) that shows better catalytic activity towards fuel cell reactions than commercial Pd/C, so the designed catalyst can act as a promising catalyst for generating biofuel cells and helps in reducing the environmental pollution.

Chapter 5

Scope of further investigation

Electrocatalysts have recently been developed rapidly, showing enhanced electrocatalytic performance for fuel cell reactions and replacing the utility Pt-based electrocatalysts, especially in alkaline media. In the case of supported noble metal catalysts, many factors, like their size, shape, and composition, can affect their catalytic behaviour. Among these factors, the morphology of the metal nanostructure, the nature of the support and metal-support interactions, and the chemical states of the metal surface are widely investigated.

It was observed that heterogeneous Pd-based electrocatalysts lack product selectivity compared to homogeneous catalysts. We can enhance their product selectivity by modifying their surface structure or electronic properties. We can tune the electronic properties of Pd-based catalysts by decorating noble metals like Pd onto various heteroatom-doped carbon materials such as B, P, S, or N. It has been predicted that metal-to-substrate charge-transfer interactions play a vital role in regulating the activity of the catalyst material.

The efficacy and product selectivity of the catalyst towards electron-donating or electron-withdrawing substrates can be improved by choosing a suitable type of element to be doped on the support carbon framework. There are several benefits of using graphene-based materials as support material in improving catalyst activity and stability because of enhanced catalyst surface area due to the anchoring of metal in crystal defects of graphene. The binding of metal on the support surface becomes more potent when we use N-doped graphene oxide as a support due to the high electronegativity of nitrogen. There are several types of N-sites in the graphene framework: graphitic N (N atoms substituting C atoms), pyridinic N (double coordinated N atom in a hexagon ring), and pyrrolic N (N atoms in a five-membered ring), and each of these N-sites influences the metal-support interactions differently. It was already observed that in the framework of NrGO, the hybridization of the sp^2 dangling bonds and metal d-orbitals leads to a pronounced charge transfer, and this charge transfer, in turn, plays a role in deciding the

catalytic ability of the material. We can further investigate this charge transfer mechanism in the designed catalyst in detail by XPS (X-ray photoelectron spectroscopy) studies.

References

- [1] Wolfram, C.; Shelef, O.; Gertler, P. How Will Energy Demand Develop in the Developing World? *J Econ Perspect.* **2012**, 26 (1), 119–138. DOI: <https://doi.org/10.1257/jep.26.1.119>.
- [2] Socolow, R.; Hotinski, R.; Greenblatt, J. B.; Pacala, S. Solving the Climate Problem: Technologies Available to Curb CO₂ Emissions. *Environment.* **2004**, 46, 8–19.
- [3] W.R. W. Daud, R. E. Rosli, E. H. Majlan, S.A.A. Hamid, R. Mohamed and T. Husain, *Renew. Energy*, **2017**, 113, 620-638.
- [4] R.E. Rosli, A.B. Sulong, W.R.W. Daud, M.A. Zulkifley, T. Husaini, M.I. Rosli, E.H. Majlan and M.A. Haque, *Int. J. Hydrogen Energy*, **2017**, 42, 9293-9314.
- [5] S. Gottesfeld, D.R. Dekel, M. Page, C. Bae, Y. Yan, P. Zelenay and Y.S. Kim, *J. Power Sources*, **2018**, 375, 170-184.
- [6] Astruc, Didier, Feng Lu, and Jaime Ruiz Aranzaes. "Nanoparticles as recyclable catalysts: the frontier between homogeneous and heterogeneous catalysis." *Angewandte Chemie International Edition* 44.48 (2005): 7852-7872.
- [7] Somorjai, G.A., F. Tao, and J.Y. Park, the nanoscience revolution: Merging of colloid science, catalysis and nanoelectronics. *Topics in Catalysis*, **2008**, 47(1U2): p.1U14
- [8] Y.N. Xia, et al. *Angew. Chem. Int. Ed.*, 47 (2008), pp. 2-46
- [9] S.J. Guo, E.K. Wang *Nano Today*, 6 (2011), pp. 240-264
- [10] Li, J., Zhao, T., Chen, T., Liu, Y., Ong, C. N., & Xie, J. (2015). Engineering noble metal nanomaterials for environmental applications. *Nanoscale*, 7(17), 7502-7519.
- [11] Kenneth J. Klabunde, Jane Stark, Olga Koper, Cathy Mohs, Dong G. Park, Shawn Decker, Yan Jiang, Isabelle Lagadic, and Dajie Zhang. *The Journal of Physical Chemistry* **1996** 100 (30), 12142-12153 DOI: 10.1021/jp960224x
- [12] Guo, Shaojun, and Erkang Wang. "Noble metal nanomaterials: controllable synthesis and application in fuel cells and analytical sensors." *Nano today* 6.3 (2011): 240-264.

- [13] Toropov, Nikita, and Tigran Vartanyan. "1.03 Noble Metal Nanoparticles: Synthesis and Optical Properties." *Comprehensive Nanoscience and Nanotechnology* (2019): 61.
- [14] Liu, Mengmeng, et al. "Recent advances in noble metal catalysts for hydrogen production from ammonia borane." *Catalysts* 10.7 (2020): 788.
- [15] Ludwig, Jacob R., and Corinna S. Schindler. "Catalyst: sustainable catalysis." *Chem* 2.3 (2017): 313-316.
- [16] Dresselhaus, M.S. and I.L. Thomas, Alternative energy technologies. *Nature*, 2001. 414(6861): p. 332-337.
- [17] Steele, B.C.H. and A. Heinzl, Materials for fuel cell technologies. *Nature*, 2001. 414(6861): p. 345-352.
- [18] Winter, M. and R.J. Brodd, what are batteries, fuel cells, and supercapacitors? *Chemical Reviews*, 2004. 104(10): p. 4245-4269.
- [19] McCreery, R.L., Advanced carbon electrode materials for molecular electrochemistry. *Chemical Reviews*, 2008. 108(7): p. 2646-2687.
- [20] Salahdin, Omar Dheyauldeen, et al. "Graphene and carbon structures and nanomaterials for energy storage." *Applied Physics A* 128.8 (2022): 703.
- [21] T. S. Zhao, R. Chen, W. W. Yang, C. Xu, *J. Power Sources* 2009, 191, 185.
- [22] B. C. Ong, S. K. Kamarudin, S. Basri, *Int. J. Hydrogen Energy* 2017, 42, 10142.
- [23] S. Kakaç, A. Pramanjaroenkij, X. Y. Zhou, *Int. J. Hydrogen Energy* 2007, 32, 761.
- [24] Hanif S, Iqbal N, Shi X, Noor T, Ali G, Kannan AM. NiCo-Ndoped carbon nanotubes-based cathode catalyst for the alkaline membrane fuel cell. *Renew Energy*. 2020;154:508-516.
- [25] Wang L, Yuan Z, Wen F, Cheng Y, Zhang Y, Wang G. A bipolar passive DMFC stack for portable applications. *Energy*. 2018;144:587-593.
- [26] Guo, Shaojun, and Erkang Wang. "Noble metal nanomaterials: controllable synthesis and application in fuel cells and analytical sensors." *Nano today* 6.3 (2011): 240-264.
- [27] Shrivastava NK, Thombre SB, Chadge RB. Liquid feed passive direct methanol fuel cell: challenges and recent advances. *Ionics*. 2016;22:1-23.

- [28] Yaqoob L, Noor T, Iqbal N, et al. Nanocomposites of cobalt benzene tricarboxylic acid MOF with rGO: an efficient and robust electrocatalyst for oxygen evolution reaction (OER). *Renew Energy*. **2020**;156:1040-1054.
- [29] Gwak G, Lee K, Ferekh S, Lee S, Ju H. Analyzing the effects of fluctuating methanol feed concentration in active-type direct methanol fuel cell (DMFC) systems. *Int J Hydrogen Energy*. **2015**;40:5396-5407.
- [30] Kamarudin SK, Achmad F, Daud WRW. Overview on the application of direct methanol fuel cell (DMFC) for portable electronic devices. *Int J Hydrogen Energy*. **2009**;34:6902-6916.
- [31] Kamarudin, S. K.; Daud, W. R. W.; Ho, S. L.; Hasran, U. A. Overview on the Challenges and Developments of Micro-direct Methanol Fuel Cells (DMFC). *J. Power Sources*. **2007**, 163, 743–754. DOI: <https://doi.org/10.1016/j.jpowsour.2006.09.081>.
- [32] K FÖGER,2 - Materials basics for fuel cells, Michael Gasik, In Woodhead Publishing Series in Electronic and Optical Materials, Materials for Fuel Cell,**2008**, Pages 6-63, ISBN 9781845693305,<https://doi.org/10.1533/9781845694838.6>.
- [33] L. Jiang, G. Sun, FUEL CELLS – DIRECT ALCOHOL FUEL CELLS | Direct Ethanol Fuel Cells,Encyclopedia of Electrochemical Power Sources,Elsevier,**2009**,Pages 390-401,<https://doi.org/10.1016/B978-044452745-5.00245-8>.
- [34] Alexandra M.F.R. Pinto, Vânia B. Oliveira and Daniela S. Falcão,Direct Alcohol Fuel Cells for Portable Applications,**2018**,<https://doi.org/10.1016/C2016-0-00632-0>.
- [35] Nabila A. Karim, Siti Kartom Kamarudin, Chapter 2 - Introduction to direct alcohol fuel cells (DAFCs),Direct Liquid Fuel Cells,Academic Press,**2021**,Pages 49-70,ISBN 9780128186244,<https://doi.org/10.1016/B978-0-12-818624-4.00002-9>.
- [36] Yaqoob, Lubna, Tayyaba Noor, and Naseem Iqbal. "A comprehensive and critical review of the recent progress in electrocatalysts for the ethanol oxidation reaction." *RSC advances* 11.27 (2021): 16768-16804.
- [37] Govindarasu, R., and S. Somasundaram. "Studies on influence of cell temperature in direct methanol fuel cell operation." *Processes* 8.3 (2020): 353.
- [38] G-energy Technologies, www.g-energy.com.
- [39] G. A. Camara and T. Iwasita, *J. Electroanal. Chem.* 578, 315 (2005).

- [40] H. Wang, Z. Jusys, and R. J. Behm, *J. Phys. Chem. B* 108, 19413 (2004).
- [41] Lai, S.C.S.; Koper, M.T.M. Ethanol electro-oxidation on platinum in alkaline media. *Phys. Chem. Chem. Phys.* 2009, 11, 10446–10456.
- [42] Wala, Marta, and Wojciech Simka. "Effect of anode material on electrochemical oxidation of low molecular weight alcohols—A review." *Molecules* 26.8 (2021): 2144.
- [43] Yaqoob, Lubna, Tayyaba Noor, and Naseem Iqbal. "Recent progress in development of efficient electrocatalyst for methanol oxidation reaction in direct methanol fuel cell." *International Journal of Energy Research* 45.5 (2021): 6550-6583.
- [44] Tong, Yueyu, et al. "Metal-based electrocatalysts for methanol electro-oxidation: progress, opportunities, and challenges." *Small* 17.9 (2021): 1904126
- [45] Tian, Xinlong, et al. "Advanced electrocatalysts for the oxygen reduction reaction in energy conversion technologies." *Joule* 4.1 (2020): 45-68.
- [46] Khotseng, Lindiwe. 'Oxygen Reduction Reaction'. *Electrocatalysts for Fuel Cells and Hydrogen Evolution - Theory to Design*, IntechOpen, Dec. 2018. Crossref, doi:10.5772/intechopen.79098.
- [47] Razumney, Wroblowa HS Yen-Chi-Pan. "G. Electroreduction of Oxygen: A New Mechanistic Criterion." *J. Electroanal. Chem. Interfacial Electrochem* 69 (1976): 195-201.
- [48] Marinkovic, N.S.; Li, M.; Adzic, R.R. Pt-Based Catalysts for Electrochemical Oxidation of Ethanol. *Top. Curr. Chem.* 2019, 377, 11.
- [49] Huang, D.-B.; Yuan, Q.; He, P.-L.; Wang, K.; Wang, X. A facile and general strategy for the synthesis of porous flowerlike Pt-based nanocrystals as effective electrocatalysts for alcohol oxidation. *Nanoscale* 2016, 8, 14705–14710.
- [50] Zheng, Y.; Wan, X.; Cheng, X.; Cheng, K.; Dai, Z.; Liu, Z. Advanced Catalytic Materials for Ethanol Oxidation in Direct Ethanol Fuel Cells. *Catalysts* 2020, 10, 166. <https://doi.org/10.3390/catal10020166>
- [51] W. Huang, X.-Y. Ma, H. Wang, R. Feng, J. Zhou, P. N. Duchesne, P. Zhang, F. Chen, N. Han, F. Zhao, J. Zhou, W.-B. Cai, Y. Li, *Adv. Mater.* 2017, 29, 1703057.

- [52] Jia F, Wong K-w, Du R. Direct growth of highly catalytic palladium nanoplates array onto gold substrate by a template-free electrochemical route. *Electrochem Commun.* **2009**;11:519-521.
- [53] Yin Z, Zheng H, Ma D, Bao X. Porous palladium nanoflowers that have enhanced methanol electro-oxidation activity. *J Phys Chem C.* **2009**;113:1001-1005.
- [54] Zhu Y, Kang Y, Zou Z, et al. Facile preparation of carbon-supported Pd nanoparticles for electrocatalytic oxidation of formic acid. *Fuel Cells Bullet.* **2008**;2008:12-15.
- [55] Zhang X, Zhu J, Tiwary CS, et al. Palladium nanoparticles supported on nitrogen and sulfur dual-doped graphene as highly active electrocatalysts for formic acid and methanol oxidation. *ACS Appl Mater Interfaces.* **2016**;8:10858-10865.
- [56] D. H. Guo, R. Shibuya, C. Akiba, S. Saji, T. Kondo, J. Nakamura, *Science* **2016**, 351, 361–365.
- [57] Zhang, Zheye, et al. "Facile synthesis of N-doped porous carbon encapsulated bimetallic PdCo as a highly active and durable electrocatalyst for oxygen reduction and ethanol oxidation." *Journal of Materials Chemistry A* 5.22 (2017): 10876-10884.
- [58] Sahoo, L., Mondal, S., Gloskovskii, A., Chutia, A., & Gautam, U. K. (2021). Unravelling charge-transfer in Pd to pyrrolic-N bond for superior electrocatalytic performance. *Journal of Materials Chemistry A*, 9 (17), 10966-10978.
- [59] S. Niu, S. Li, Y. Du, X. Han and P. Xu, *ACS Energy Lett.*, **2020**, 5, 1083–1087.
- [60] Y.Garsany,O.A.Baturina,K.E.Swider-Lyons and S.S.Kocha,*Anal.Chem.*,**2010**,82,6321-6328.
- [61] Habibullah, G.; Viktorova, J.; Ruml, T. Current Strategies for Noble Metal Nanoparticle Synthesis. *Nanoscale Res. Lett.* **2021**, 16, 47
- [62] Herizchi, R.; Abbasi, E.; Milani, M.; Akbarzadeh, A. Current methods for synthesis of gold nanoparticles. *Artif. Cells Nanomed. Biotechnol.* **2016**, 44, 596–602.
- [63] Karczmarzka, Agnieszka, et al. "Carbon-Supported Noble-Metal Nanoparticles for Catalytic Applications—A Review." *Crystals* 12.5 (2022): 584.

- [64] Reverberi, A.; Kuznetsov, N.; Meshalkin, V.; Salerno, M.; Fabiano, B. Systematical analysis of chemical methods in metal nanoparticles synthesis. *Theor. Found. Chem. Eng.* **2016**, *50*, 59–66.
- [65] Silva, L.I.; Perez-Gramatges, A.; Larrude, D.G.; Almeida, J.M.; Aucélio, R.Q.; da Silva, A.R. Gold nanoparticles produced using NaBH₄ in absence and in the presence of one-tail or two-tail cationic surfactants: Characteristics and optical responses induced by aminoglycosides. *Colloids Surfaces Physicochem. Eng. Asp.* **2021**, *614*, 126174.
- [66] Moonrat, C.; Kittinaovarut, S.; Jinawath, S.; Sujaridworakun, P. The Effect of pH Values on Color Development of Silver Colloids. In *Key Engineering Materials*; Trans Tech Publications Ltd.: Freienbach, Switzerland, **2020**; Volume 862, pp. 17–21.
- [67] Mehr, F.P.; Khanjani, M.; Vatani, P. Synthesis of nano-Ag particles using sodium borohydride. *Orient. J. Chem.* **2015**, *31*, 1831–1833.
- [68] Sudirman, S.; Adi, W.A.; Budianto, E.; Yudianti, R. Mono-Dispersed Pt/MWNTs: Growing Directly on Multiwall Carbon Nanotubes (MWNTs) Using NaBH₄ as Reducing Agent for Component of Proton Exchange Membrane Fuel Cell (PEMFC). *Int. J. Chem.* **2020**, *12*, 37–48.
- [69] Jung, S.C.; Park, Y.K.; Jung, H.Y.; Kim, S.C. Effect of Stabilizing Agents on the Synthesis of Palladium Nanoparticles. *J. Nanosci. Nanotechnol.* **2017**, *17*, 2833–2836.
- [70] Sharma, Surbhi, and Bruno G. Pollet. "Support materials for PEMFC and DMFC electrocatalysts—A review." *Journal of Power Sources* 208 (**2012**): 96-119.
- [71] Y. Shao, J. Sui, G. Yin and Y. Gao, *Appl. Catal., B*, **2008**, *79*, 89–99.
- [72] Sahoo, L., Mondal, S., Gloskovskii, A., Chutia, A., & Gautam, U. K. (**2021**). Unravelling charge-transfer in Pd to pyrrolic-N bond for superior electrocatalytic performance. *Journal of Materials Chemistry A*, *9*(17), 10966-10978.
- [73] Zhang, Xin, et al. "Palladium nanoparticles supported on nitrogen and sulfur dual-doped graphene as highly active electrocatalysts for formic acid and methanol oxidation." *ACS applied materials & interfaces* *8*.17 (**2016**): 10858-10865.
- [74] Z. R. Yang , S. Q. Wang , J. Wang , A. J. Zhou and C. W. Xu , *Sci. Rep.*, **2017**, *7* , 1 —8.

- [75] Y. Wang , Q. He , J. Guo , J. Wang , Z. Luo and T. D. Shen , *ACS Appl. Mater. Interfaces*, **2015**, **7** , 23920 —23931.
- [76] K. S. Bhavani , T. Anusha , J. S. Kumar and P. K. Brahman , *Electroanalysis*, **2021**, **33** , 97 —110.
- [77] Q. Dong , Y. Zhao , X. Han , Y. Wang , M. Liu and Y. Li , *Int. J. Hydrogen Energy*, **2014**, **39** , 14669 —14679.
- [78] A. R. Rajamani , P. Ashly , L. Dheer , S. C. Sarma , S. Sarkar and D. Bagchi , *ACS Appl. Energy Mater.*, **2019**, **2** , 7132 —7141.
- [79] G. Hu , F. Nitze , H. R. Barzegar , T. Sharifi , A. Mikołajczuk and C. W. Tai , *J. Power Sources*, **2012**, **209** , 236 —242.
- [80] S. Sarkar , R. Jana , U. V. Waghmare , B. Kuppan , S. Sampath and S. C. Peter , *Chem. Mater.*, **2015**, **27** , 7459 —7467.
- [81] C. Peng , Y. Hu , M. Liu and Y. Zheng , *J. Power Sources*, **2015**, **278** , 69 —75.
- [82] L. L. Sikeyi , T. Matthews , A. S. Adekunle and N. W. Maxakato , *Electroanalysis*, **2020**, **32** , 2681 —2692.
- [83] Mandal K, Bhattacharjee D, Roy PS, Bhattacharya SK, Dasgupta S. Room temperature synthesis of Pd–Cu nanoalloy catalyst with enhanced electrocatalytic activity for the methanol oxidation reaction. *Appl Catal Gen.* **2015**;492:100-106.
- [84] Zhang K, Xiong Z, Li S, Yan B, Wang J, Du Y. Cu₃P/RGO promoted Pd catalysts for alcohol electro-oxidation. *J Alloys Compd.* **2017**;706:89-96.
- [85] Niu X, Zhao H, Lan M. Palladium deposits spontaneously grown on nickel foam for electro-catalyzing methanol oxidation: effect of precursors. *J Power Sources.* **2016**;306:361-368.
- [86] D.-X. Yu et.al, *Electrochem. Acta*, **2016**, 213, 565–573.
- [87] Hosseini M, Momeni M, Khalilpur H. Synthesis and characterization of palladium nanoparticles immobilized on TiO₂ nanotubes as a new high active electrode for methanol electro-oxidation. *Int J Nanoscience.* **2012**;11:1250016.
- [88] L. Chao et. al, *Int. J. Hydrogen Energy*, **2017**, 42, 15107–15114.

[89] K. Wu, Q. et.al, *Int. J. Hydrogen Energy*, **2015**, 40, 6530–6537.

[90] C. He, J. Tao, G. He and P. K. Shen, *Electrochem. Acta*, **2016**, 216, 295–303.

[91] Gao L, Yue W, Tao S, Fan L. Novel strategy for preparation of graphene-Pd, Pt composite, and its enhanced electrocatalytic activity for alcohol oxidation. *Langmuir*. **2013**;29:957-964.